

1  
2  
3  
4

## 5 **Title:** Cortico-Fugal Regulation of Predictive Coding.

6  
7  
8  
9

**Authors:** Alexandria M.H. Lesicko<sup>1</sup>, Christopher F. Angeloni<sup>2</sup>, Jennifer M. Blackwell<sup>3</sup>, Mariella De Biasi<sup>4,5,6</sup>, Maria N. Geffen<sup>1,6,7</sup>

## 10 *Affiliations:*

- 11 1. Department of Otorhinolaryngology, University of Pennsylvania, Philadelphia, United States  
12 2. Department of Psychology, University of Pennsylvania, Philadelphia, United States  
13 3. Department of Neurobiology and Behavior, Stony Brook University, Stony Brook, New York,  
14 United States  
15 4. Department of Psychiatry, University of Pennsylvania, Philadelphia, United States  
16 5. Department of Systems Pharmacology and Experimental Therapeutics, University of  
17 Pennsylvania, Philadelphia, United States  
18 6. Department of Neuroscience, University of Pennsylvania, Philadelphia, United States  
19 7. Department of Neurology, University of Pennsylvania, Philadelphia, United States

## 22 *Corresponding author*

Dr. Maria N. Geffen  
Stemmler Hall G10  
3450 Hamilton Walk  
Philadelphia, PA 19104  
(215)898-0872  
[mgeffen@pennmedicine.upenn.edu](mailto:mgeffen@pennmedicine.upenn.edu)

**Keywords:** prediction error, hierarchical predictive coding, inferior colliculus, auditory cortex, cortico-collicular, stimulus specific adaptation, deviance detection

31 ABSTRACT

32 Sensory systems must account for both contextual factors and prior experience to adaptively engage  
33 with the dynamic external environment. In the central auditory system, neurons modulate their  
34 responses to sounds based on statistical context. These response modulations can be understood  
35 through a hierarchical predictive coding lens: responses to repeated stimuli are progressively  
36 decreased, in a process known as repetition suppression, whereas unexpected stimuli produce a  
37 prediction error signal. Prediction error incrementally increases along the auditory hierarchy from the  
38 inferior colliculus (IC) to the auditory cortex (AC), suggesting that these regions may engage in  
39 hierarchical predictive coding. A potential substrate for top-down predictive cues is the massive set  
40 of descending projections from the auditory cortex to subcortical structures, although the role of this  
41 system in predictive processing has never been directly assessed. We tested the effect of optogenetic  
42 inactivation of the auditory cortico-collicular feedback in awake mice on responses of IC neurons to  
43 stimuli designed to test prediction error and repetition suppression. Inactivation of the cortico-  
44 collicular pathway led to a decrease in prediction error in IC. Repetition suppression was unaffected  
45 by cortico-collicular inactivation, suggesting that this metric may reflect fatigue of bottom-up sensory  
46 inputs rather than predictive processing. We also discovered populations of IC neurons that exhibit  
47 repetition enhancement, a sequential increase in firing with stimulus repetition. Cortico-collicular  
48 inactivation led to a decrease in repetition enhancement in the central nucleus of IC, suggesting that  
49 it is a top-down phenomenon. Negative prediction error, a stronger response to a tone in a predictable  
50 rather than unpredictable sequence, was suppressed in shell IC units during cortico-collicular  
51 inactivation. These changes in predictive coding metrics arose from bidirectional modulations in the  
52 response to the standard and deviant contexts, such that neurons in IC responded more similarly to  
53 each context in the absence of cortical input. We also investigated how these metrics compare  
54 between the anesthetized and awake states by recording from the same neurons under both conditions.  
55 We found that metrics of predictive coding and deviance detection differ depending on the anesthetic  
56 state of the animal, with negative prediction error emerging in the central IC and repetition  
57 enhancement and prediction error being more prevalent in the absence of anesthesia. Overall, our  
58 results demonstrate that the auditory cortex provides cues about the statistical context of sound to  
59 subcortical brain regions via direct feedback, regulating processing of both prediction and repetition.

## 60 INTRODUCTION

61 Sensory systems differentially encode environmental stimuli depending on the context in  
62 which they are encountered (De Franceschi & Barkat, 2020; Herrmann et al., 2015; Jaramillo et al.,  
63 2014; Pakan et al., 2016; Takesian et al., 2018; Zhai et al., 2020). The same physical stimulus can  
64 elicit distinct neuronal responses depending on whether it is predictable or unexpected in a given  
65 sensory stream (Weissbart et al., 2020; Yaron et al., 2012). One framework for understanding this  
66 dynamic sensory capability is hierarchical predictive coding, which suggests that neuronal networks  
67 form predictions about incoming stimuli based on the statistics of prior experience (Friston & Kiebel,  
68 2009). These predictions are generated at higher levels of the sensory hierarchy and broadcast to  
69 lower stations to minimize processing of redundant input and maximize coding efficiency (Friston,  
70 2009; Friston & Kiebel, 2009). Any mismatch between predictions and representations of sensory  
71 input is coded in a neuronal response known as a “prediction error”, which is further propagated up  
72 the sensory hierarchy, ultimately allowing for the formation of updated predictions (Friston & Kiebel,  
73 2009; Shipp, 2016). Multiple sensory modalities exhibit hierarchical predictive coding, including the  
74 motor, visual, and auditory systems (Okada et al., 2018; Parras et al., 2017; Rao & Ballard, 1999;  
75 Rauss et al., 2011; Schellekens et al., 2016; Shipp et al., 2013).

76 Neurons in select regions of the central auditory system are sensitive to statistical context,  
77 responding more strongly to a tone when it is presented rarely (a “deviant”) than when it is  
78 commonplace (a “standard”) (Ulanovsky et al., 2003). This phenomenon, known as stimulus specific  
79 adaptation (SSA), is prevalent in the auditory cortex (Natan et al., 2015; Ulanovsky et al., 2003).  
80 Weaker SSA is present in regions peripheral to the AC, including the auditory midbrain, or inferior  
81 colliculus (IC), and the auditory thalamus, or medial geniculate body (MGB) (Anderson et al., 2009;  
82 Antunes et al., 2010; Duque & Malmierca, 2015; Malmierca et al., 2009; Taaseh et al., 2011;  
83 Ulanovsky et al., 2003). Subdivisions in IC and MGB that receive descending projections from AC  
84 exhibit relatively higher SSA levels than their lemniscal counterparts (Antunes et al., 2010; Duque et  
85 al., 2012), suggesting that SSA may be generated de novo in AC and subsequently broadcast to  
86 subcortical structures via cortico-fugal projections (Nelken & Ulanovsky, 2007). Silencing of AC  
87 through cooling has been shown to modulate, but not abolish, SSA in IC and MGB of anesthetized  
88 rats (Anderson & Malmierca, 2013; Antunes & Malmierca, 2011). However, it remains unknown  
89 whether these modulations in the SSA index with cortical deactivation reflect changes in predictive  
90 processing.

91 Recent studies have implemented additional control tone sequences to further decompose the  
92 traditional SSA index into two distinct underlying processes: repetition suppression and prediction

93 error (Harms et al., 2014; Parras et al., 2017; Ruhnau et al., 2012). Repetition suppression is  
94 characterized by a decrease in firing rate to each subsequent presentation of a standard tone  
95 (Auksztulewicz & Friston, 2016; Parras et al., 2017). Prediction error is thought to signal the  
96 mismatch between the predicted input, based on prior experience with repeated presentations of the  
97 standard, and the actual sensory input when a deviant tone is presented (Friston, 2009; Friston &  
98 Kiebel, 2009). Whereas repetition suppression is thought to potentially reflect synaptic depression,  
99 prediction error has been proposed to underlie true deviance detection (Parras et al., 2017; Taaseh et  
100 al., 2011). Prediction error increases along the auditory hierarchy and is more prevalent in regions of  
101 IC and MGB that receive cortical feedback (Parras et al., 2017), suggesting that these subcortical  
102 regions may engage in hierarchical predictive coding, with AC potentially providing predictive cues  
103 to IC and MGB. However, how feedback projections from AC shape predictive processing in  
104 subcortical targets has never been directly assessed. In fact, virtually all models of hierarchical  
105 predictive coding to date have focused on intra-cortical connections, with the massive system of  
106 descending cortico-fugal projections remaining unexplored (Asilador & Llano, 2020; Bastos et al.,  
107 2012).

108 Here, we investigated how inputs from AC to IC, the first station in the auditory system in  
109 which prediction error is found, shape metrics associated with predictive coding and deviance  
110 detection (Parras et al., 2017). To test this, we optogenetically inactivated cortico-collicular feedback  
111 while recording neuronal responses in IC and found that prediction error, negative prediction error,  
112 and repetition enhancement in IC are altered in the absence of cortical input. Our results suggest that  
113 the cortico-collicular pathway sends cues from AC to IC regarding the statistical context of auditory  
114 stimuli.

115 RESULTS

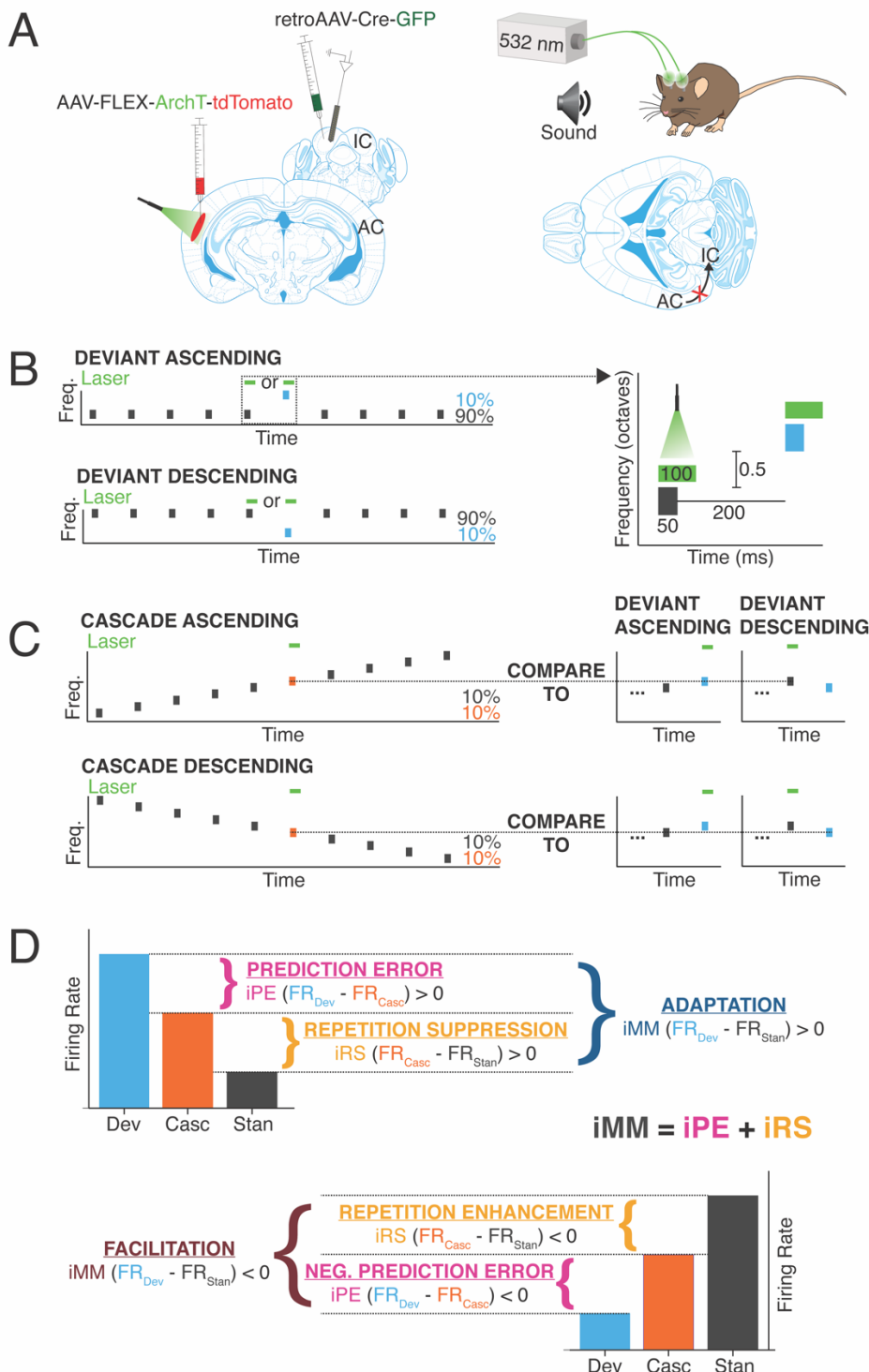
116 *Experimental design*

117 We used a Cre/FLEX viral injection strategy to selectively express the inhibitory opsin,  
118 ArchT, in cortico-collicular neurons of four mice by injecting a retroAAV-Cre-GFP construct into IC  
119 and an AAV9-FLEX-ArchT-tdTomato construct into AC (Figure 1A, left). The retroAAV-Cre-GFP  
120 construct is transported in a retrograde fashion and expressed in neurons that project to IC (Blackwell  
121 et al., 2020). The genes encoded in the AAV9-FLEX-ArchT-tdTomato construct can only be  
122 expressed in neurons containing the Cre construct, thereby limiting ArchT expression to neurons in  
123 AC that project to IC. In the presence of green light, ArchT, a light-driven outward proton pump,  
124 mediates rapid, reversible inactivation of the neurons in which it is expressed (Han et al., 2011).

125 We implanted cannulas over AC in mice injected with the Cre/FLEX constructs and a 532 nm  
126 laser was used to provide green light illumination to the region, allowing for inactivation of cortico-  
127 collicular neurons (Figure 1A, right). The mice were head-fixed and a 32-channel probe was lowered  
128 into IC to perform awake extracellular recordings (Figure 1A). Auditory stimuli consisted of oddball  
129 sequences of two repeated pure tones, presented at a 90:10 standard-to-deviant ratio and half-octave  
130 frequency separation (Figure 1B). On a subset of trials, presentations of either the deviant or the last  
131 standard prior to the deviant were coupled with activation of the green laser (Figure 1B, right).

132 Neurons that displayed a significantly higher response to the deviant than the standard were  
133 designated as “adapting” neurons, while those that exhibited a significantly higher response to the  
134 standard than the deviant were categorized as “facilitating” neurons (Figure 1D). The difference in  
135 firing rate to the standard and deviant was quantified with an index of neuronal mismatch (iMM),  
136 which is equivalent to the SSA index used in previous studies (Parras et al., 2017).

137 A cascade stimulus consisting of 10 evenly spaced tones, including the tone pair from the  
138 oddball sequence, was presented to further decompose the neuronal mismatch between the responses  
139 to the standard and deviant (Figure 1C, 1D). This stimulus is unique in that each tone occurs with the  
140 same likelihood as the deviant tone in the oddball stimulus (10%), but it contains no true statistical  
141 deviants: each tone has the same likelihood of presentation, and the tone sequence overall follows a  
142 regular and predictable pattern (Parras et al., 2017). Therefore, the response to a given tone when it  
143 is embedded in the cascade can be compared to the response when it is a deviant in order to isolate  
144 prediction error effects (Figure 1C; 1D, top). A neuron exhibits prediction error if it fires more  
145 strongly to a tone when it is a deviant than when it is presented in the cascade sequence (Figure 1D,  
146 top). Conversely, if a neuron responds more strongly to a tone presented in the cascade sequence than  
147



148  
149 Figure 1: Experimental design. A) Cre/FLEX dual injections for selective ArchT expression in cortico-collicular neurons. Recordings  
150 were performed in IC while inactivation was mediated by a 532 nm laser connected to cannulas implanted over AC. B) Oddball  
151 stimuli consisted of pairs of pure tones separated by 0.5 octave with a 90:10 standard-to-deviant ratio. Two sequences were  
152 constructed such that each frequency is represented as both the standard and the deviant. C) Cascade sequences consisted of 10  
153 evenly spaced tones separated by 0.5 octaves, with both frequencies from the oddball sequence included in the sequence. Responses  
154 to tones in the cascade context were compared to responses in the standard and deviant context to analyze repetition and prediction  
155 effects, respectively. D) A positive iMM (top diagram) indicates a stronger response to the deviant than the standard (adaptation),  
156 while a negative iMM (bottom diagram) indicates a stronger response to the standard than to the deviant (facilitation). The iMM can  
157 be further decomposed into an iPE and an iRS. Positive iPE indices represent prediction error and negative values convey negative  
158 prediction error. Positive iRS indices indicate repetition suppression, while repetition enhancement is represented by negative values.

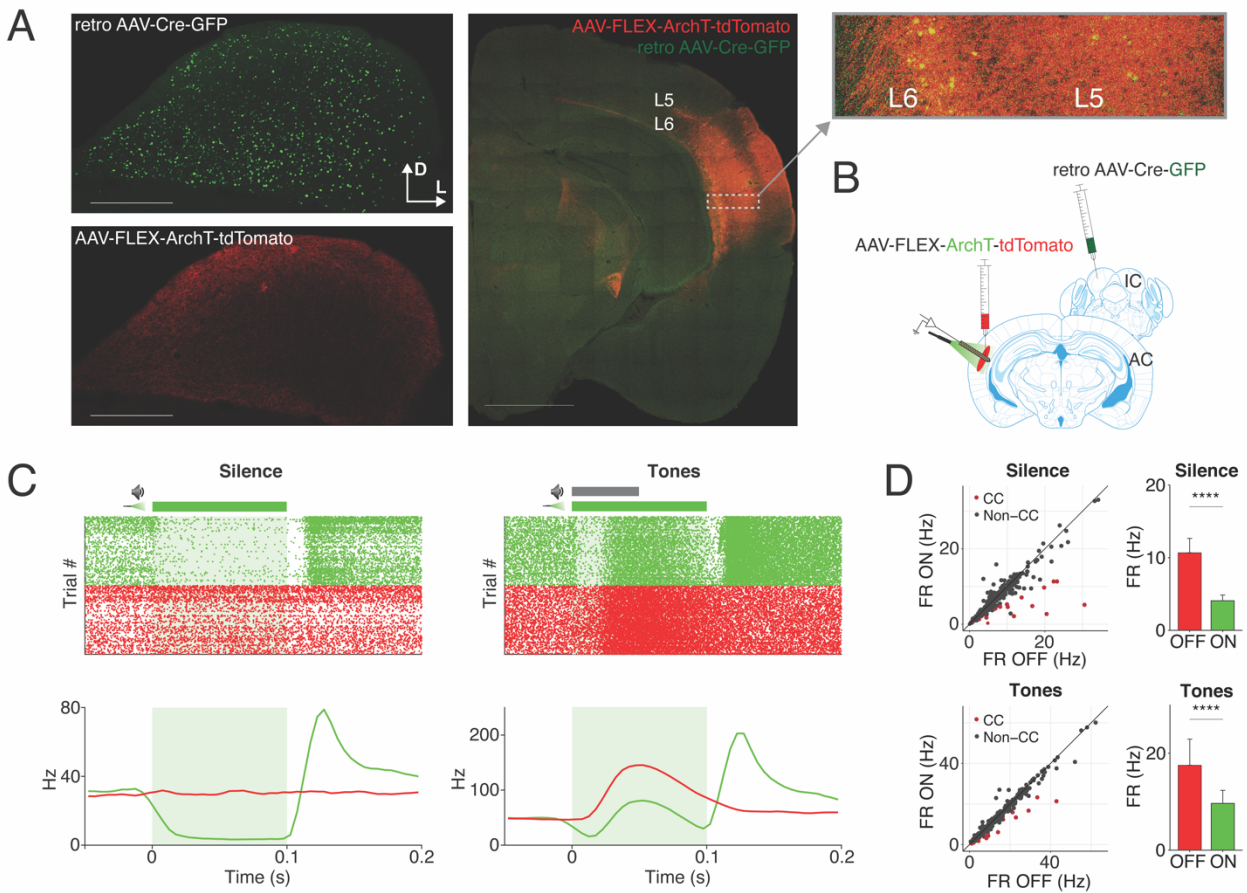
159 when it is a deviant, the neuron encodes negative prediction error (Figure 1D, bottom). This  
160 phenomenon is quantified using an index of prediction error (iPE), with positive indices indicating  
161 prediction error and negative indices representing negative prediction error (Figure 1D).

162 The cascade sequence is also free from repetition effects, since adjacent tone presentations  
163 never include a tone of the same frequency (Figure 1C). Therefore, the response to a given tone  
164 embedded in the cascade sequence can be compared to the response generated when that tone is a  
165 standard. The difference in response indicates either repetition suppression (stronger response to the  
166 tone in the cascade) (Figure 1D, top) or repetition enhancement (stronger response to the tone as a  
167 standard) (Figure 1D, bottom). These contrasting processes are quantified by the index of repetition  
168 suppression (iRS), with a positive index indicating repetition suppression and a negative index  
169 representing repetition enhancement (Figure 1D).

170  
171 *Cre/FLEX viral injection strategy enables selective inactivation of cortico-collicular neurons*

172 Examination of fixed tissue from injected mice revealed that expression of the retroAAV-Cre-  
173 GFP construct was restricted to IC (Figure 1 – Figure Supplement 1A, top left). Somatic expression  
174 of tdTomato (indicating the presence of ArchT) was restricted to layer 5 and deep layer 6 of AC,  
175 which contain cortico-collicular cell bodies, and was broadly distributed throughout the rostro-caudal  
176 extent of the auditory cortex (Figure 1 – Figure Supplement 1A, right) (Bajo et al., 2007; Schofield,  
177 2009; Yudintsev et al., 2019). Axons and terminals labeled with tdTomato were distributed in IC in  
178 a manner matching the known projection pattern of this pathway, with dense, “patchy” labeling in  
179 shell regions of IC (Figure 1 – Figure Supplement 1A, bottom left) (Herbert et al., 1991; Lesicko et  
180 al., 2016; Saldaña et al., 1996; Torii et al., 2013). These data confirm that our viral injection strategy  
181 leads to selective transfection of cortico-collicular neurons.

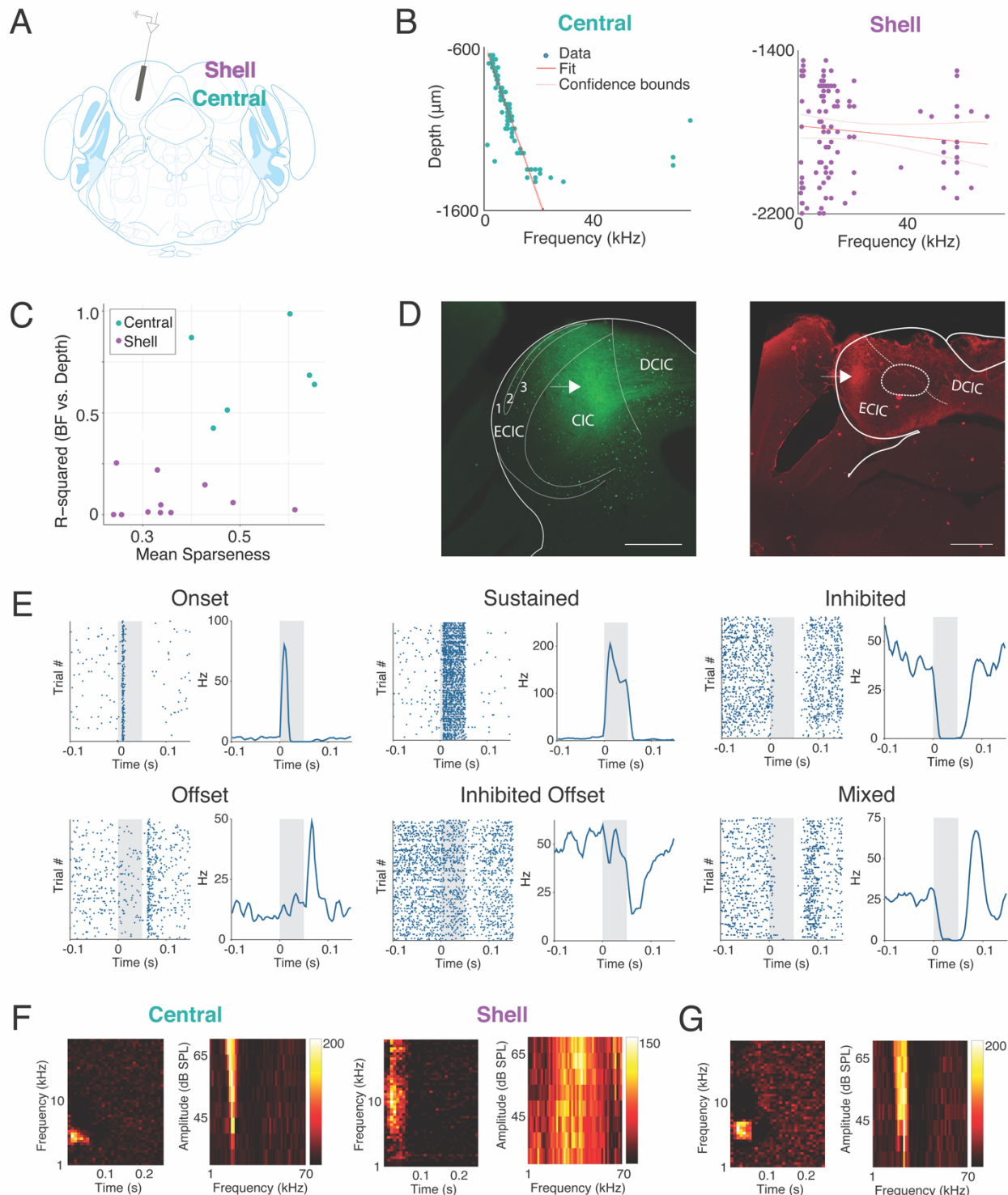
182 Extracellular recordings in AC of injected mice revealed a reduction in firing rate during the  
183 duration of the laser stimulus in several neurons (Figure 1 – Figure Supplement 1B, 2C). In these  
184 putative cortico-collicular neurons, laser-induced inactivation led to a mean ~60% reduction in firing  
185 rate at baseline (Figure 1 – Figure Supplement 1C, left; 2D, top; Table 1; p=1.9e-06, Wilcoxon signed  
186 rank test) and an average ~45% reduction in firing during presentation of pure tone stimuli (Figure 1  
187 – Figure Supplement 1C, right; 2D, bottom; Table 1; p=1.9e-06, Wilcoxon signed rank test). These  
188 results indicate that our optogenetic parameters significantly suppress cortico-collicular neurons.



189  
190 Figure 1 – Figure Supplement 1: Cre/FLEX viral injection strategy enables selective inactivation of cortico-collicular neurons. A)  
191 Expression of the retroAAV-Cre-GFP construct at the injection site is restricted to IC (top left). tdTomato labeled axons are found in  
192 a pattern matching the known topographical distribution of cortico-collicular neurons in IC (left bottom). Somatic AAV9-FLEX-  
193 ArchT-tdTomato expression is present in layer 5 and 6 of AC (right, inset). B) Experimental design for recording from AC to confirm  
194 presence of inactivated neurons. C) Example of an inactivated neuron (i.e. putative cortico-collicular neuron) exhibiting a strong  
195 reduction in firing during silence and during the presentation of pure tones. D) Population data demonstrating reduced firing rates  
196 during silence and in response to pure tone stimuli in putative cortico-collicular neurons. Dots represent individual neurons. Bar plots  
197 represent means over the population n = 20 CC neurons. Error bars are standard error of the mean.

### 198 Parsing of recording sites into central and shell locations

199 Shell and central regions of IC differ in their tuning, degree of adaptation, and amount of input  
200 from AC, and may also play distinct roles in predictive processing (Aitkin et al., 1975; Bajo et al.,  
201 2007; Blackwell et al., 2020; Duque et al., 2012; Herbert et al., 1991; Stebbings et al., 2014; Syka et  
202 al., 2000). We quantitatively parsed our recording sites by exploiting known differences in the  
203 sharpness of tuning and direction of frequency gradients between shell and central regions: shell IC  
204 neurons tend to have broader frequency tuning (low sparseness) than central IC neurons, and the  
205 central IC is characterized by a highly stereotyped tonotopic gradient with depth (Figure 1 – Figure  
206 Supplement 2A) (Aitkin et al., 1975; Chen et al., 2012; Malmierca et al., 2008; Stiebler & Ehret,  
207 1985; Syka et al., 2000). Similar to previously established procedures used in human and monkey IC  
208 research, we performed clustering analysis using the mean sparsity and variation in best frequency



209  
210 Figure 1 – Figure Supplement 2: Parsing of recording sites into central and shell locations. A) Experimental design for awake IC  
211 recordings in the central and shell regions of IC. B) Linear fits for best frequency vs. depth in central (left) and shell (right) IC. C)  
212 Sparseness vs.  $R^2$  value for linear fit. K-means clustering was performed using these parameters to classify recording sites as either in  
213 the shell or central nucleus of IC. D) Left: DiA labeling from an electrode penetration in a recording site classified as a central site.  
214 Atlas image overlay confirms that the dye track runs through the central IC (CIC) (Paxinos & Franklin, 2019). Right: DiD labeling  
215 from an electrode penetration in a recording site classified as a shell site. Atlas image overlay confirms that the dye track runs  
216 through the shell IC (here denoted as ECIC/DCIC). E) Example raster plots and peristimulus time histograms showing different firing  
217 types in the awake IC. F) Example tuning curves in central (left) and shell (right) IC. G) Example of a tuning curve with inhibited  
218 side-bands.

219 with depth from each recording site to determine whether it was from the central nucleus or shell  
220 regions of IC (Figure 1 – Figure Supplement 2B, 3C) (Bulkin & Groh, 2011; Ress & Chandrasekaran,  
221 2013). In a subset of recordings, we also marked the recording electrode with a lipophilic dye to  
222 histologically confirm the recording location (Figure 1 – Figure Supplement 2D).

223 IC neurons in both regions exhibited multiple response types to pure tone stimuli (Figure 1 –  
224 Figure Supplement 2E). In addition to excitatory responses (e.g. onset and sustained responses),  
225 inhibited and offset responses were common, as has previously been characterized in IC of awake  
226 animals (Figure 1 – Figure Supplement 2E, top right, bottom middle) (Duque & Malmierca, 2015).  
227 Consistent with previous findings, tuning curves from central regions were sharp and narrow, whereas  
228 neurons in shell regions exhibited broad frequency tuning (Figure 1 – Figure Supplement 2F, left vs.  
229 right) (Aitkin et al., 1975; Syka et al., 2000). Inhibited side-bands were common in tuning curves  
230 from both regions, and some inhibited tuning curves were observed (Figure 1 – Figure Supplement  
231 2G). These data confirm that our experimental parameters elicit sound responses and tuning properties  
232 characteristic of central and shell regions of the awake IC (Aitkin et al., 1975; Duque & Malmierca,  
233 2015; Syka et al., 2000).

234  
235 *IC neurons encode different aspects of prediction and repetition in awake and anesthetized states*

236 Much of the research regarding SSA and deviance detection in IC to date has been performed  
237 in anesthetized animals, with few studies recording from awake subjects (Duque & Malmierca, 2015;  
238 Parras et al., 2017). Given that neuronal responses to sound depend on the state of anesthesia of the  
239 subject, it is possible that there are differences in predictive coding metrics between the awake and  
240 anesthetized states (Fontanini & Katz, 2008; Gaese & Ostwald, 2001; Schumacher et al., 2011). While  
241 previous studies have characterized how anesthesia affects SSA, it remains unknown whether its  
242 component repetition and prediction metrics differ with anesthetic state (Duque & Malmierca, 2015).  
243 Therefore, we first characterized how anesthesia affects these predictive coding metrics in a subset of  
244 animals. We first performed awake recordings and then repeated our experimental procedures,  
245 leaving the animal head-fixed and the probe in place, after anesthetizing the mouse with isoflurane  
246 (Figure 2A). This protocol allowed us to compare how metrics of predictive coding differ between  
247 the awake and anesthetized preparations in the same population of neurons.

248 In the central IC, the mean iMM in the anesthetized condition was positive, indicative of  
249 prevalent adaptation (Figure 2B). The iMM values under anesthesia were significantly higher than  
250 those obtained while the animal was awake (Figure 2B, Table 1;  $p=8.8\text{e-}05$ , Wilcoxon rank sum test).  
251 To better understand what prediction or repetition effects underlie iMM in each condition, the iMM

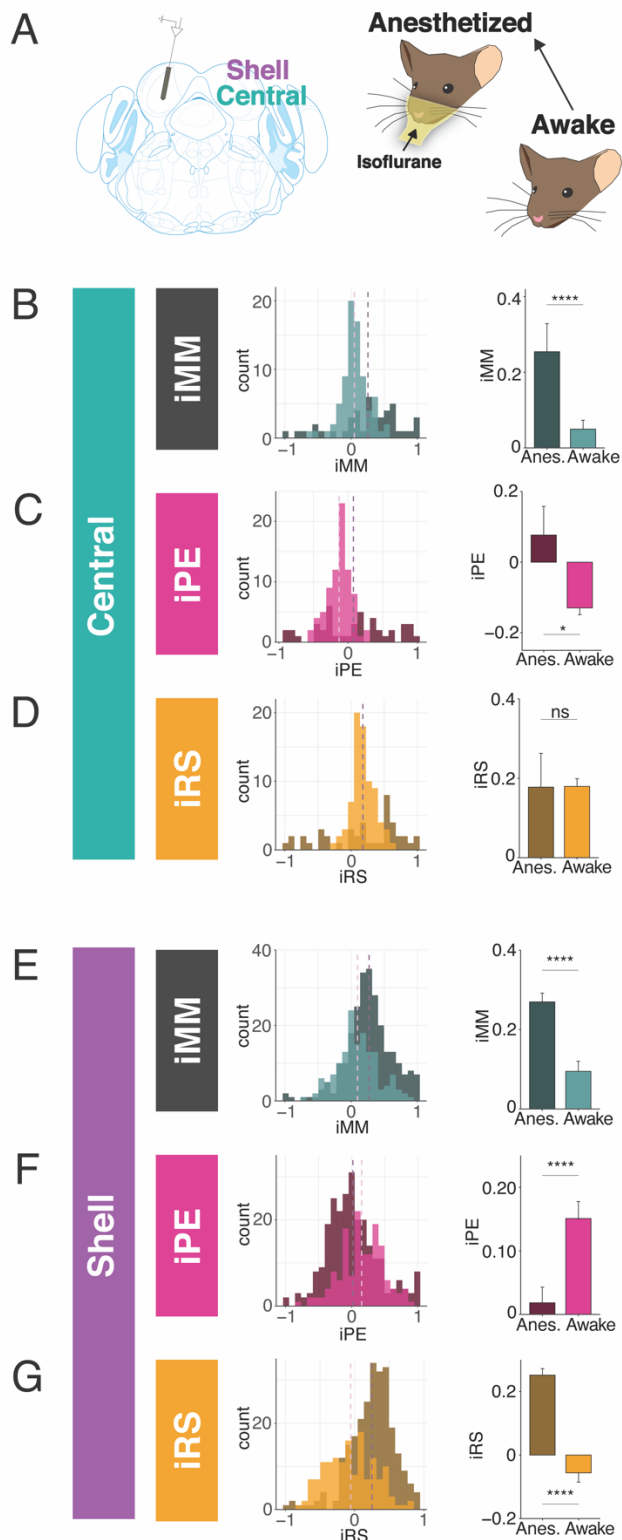
252 for both distributions was further decomposed into an iPE and iRS. In the anesthetized condition, the  
253 mean iPE value of 0.077 indicated the presence of modest prediction error, while an iPE value of -  
254 0.13 indicated that negative prediction error is significantly more prevalent in the awake condition  
255 (Figure 2C, Table 1; p=0.017, Student's T-test). Under both anesthetized and awake conditions,  
256 prominent repetition suppression was observed in the central IC (Figure 2D).

257 Similar to the central IC, the mean iMM was significantly more positive in shell regions during  
258 anesthesia (Figure 2E, Table 1; p=3.5e-08, Wilcoxon rank sum test). A greater proportion of neurons  
259 in the awake condition had a negative iMM compared with the anesthetized distribution, indicating  
260 that facilitation (a greater response to the standard than the deviant context) is more common in the  
261 awake than the anesthetized condition (Figure 2E). The iPE values in shell IC suggest that prediction  
262 error is significantly higher in the awake compared to the anesthetized condition (Figure 2F, Table 1;  
263 p=2.6e-05, Wilcoxon rank sum test). Although the distribution for the iRS under anesthesia had a  
264 positive mean of 0.25, indicating prevalent repetition suppression, the awake distribution exhibited a  
265 significant leftward shift by comparison (Figure 2G). Interestingly, the mean iRS for the awake  
266 condition was negative (mean=-0.056), indicating that repetition *enhancement*, rather than  
267 suppression, is present in the awake shell IC (Figure 2G, Table 1; p=2.5e-16, Wilcoxon rank sum  
268 test). These results point to differences between predictive coding metrics in the awake and  
269 anesthetized states, with previously undescribed metrics such as repetition enhancement and negative  
270 prediction error more prominent in awake animals.

271  
272 *Adapting and facilitating neurons are differentially affected by cortico-collicular inactivation*

273 We next performed recordings in IC of awake mice to determine how neuronal mismatch and  
274 its component repetition and prediction metrics were affected by cortico-collicular inactivation  
275 (Figure 3A). To inactivate cortico-collicular feedback, we shined light over AC in subjects which  
276 expressed a suppressive opsin in cortico-collicular neurons. We segregated the population of recorded  
277 neurons according to those that exhibited a significantly stronger response to the deviant than the  
278 standard (adapting neurons; Figure 3B, blue; 5C), those that exhibited a significantly stronger  
279 response to the standard than the deviant (facilitating neurons; Figure 3B, red; 5F), and those that  
280 responded equally to both stimulus contexts (non-adapting neurons; Figure 3B, green) for recordings  
281 in both central and shell regions of IC (Figure 3B, left vs. right).

282 The iMM for adapting neurons in the central nucleus significantly decreased with laser  
283 inactivation of cortico-collicular neurons (Figure 3D, top; Table 1; p=0.00034, Wilcoxon signed rank  
284 test). The iMM at baseline for adapting neurons predominantly represents repetition suppression

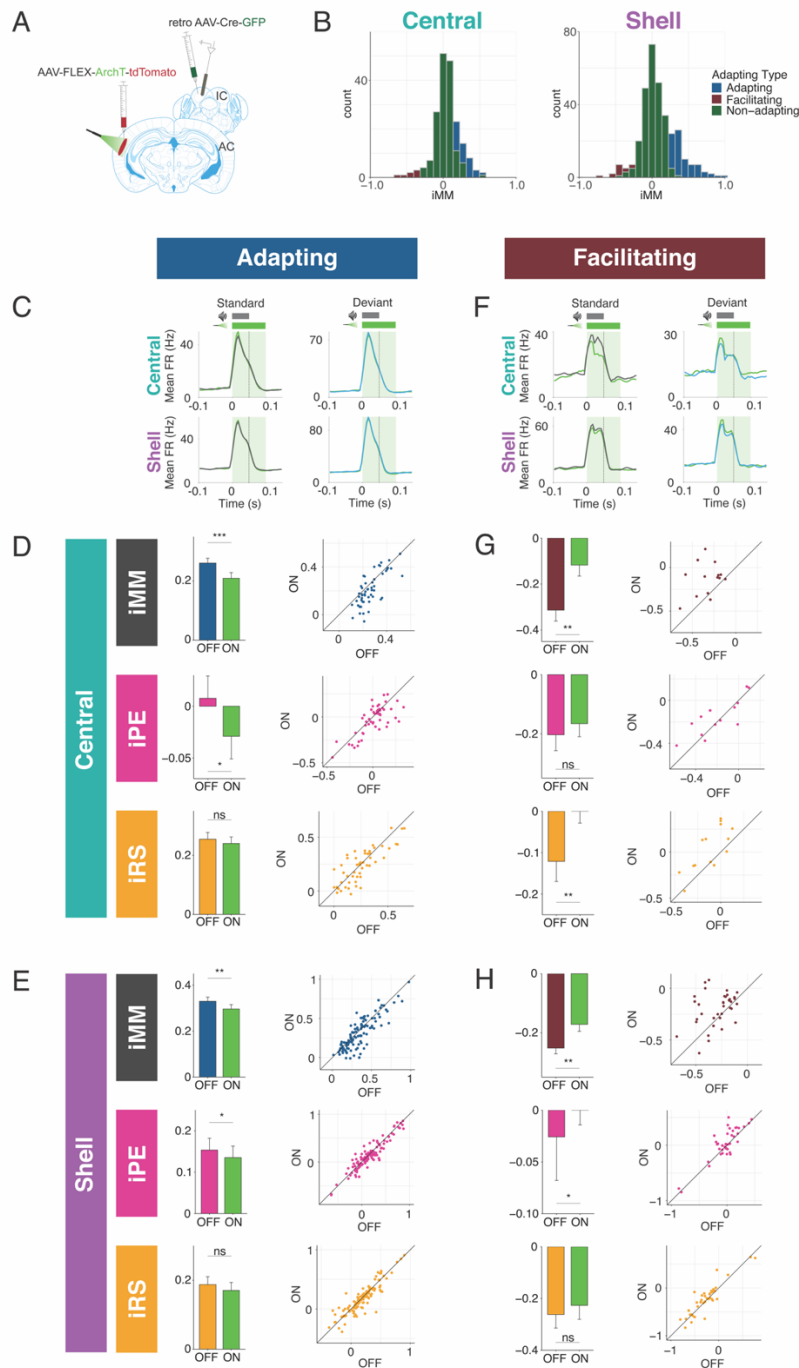


285  
 286 Figure 2: IC neurons encode different aspects of prediction and repetition in awake and anesthetized states. A) Experimental design  
 287 for recording in the awake and isoflurane anesthetized IC in the same population of neurons. B) Distribution of iMM in the awake vs.  
 288 anesthetized central IC. Bar plots represent means over the population of  $n = 39$  neurons. Error bars are standard error of the mean.  
 289 C) iPE distribution in the awake vs. anesthetized central IC. D) iRS distribution in the awake vs. anesthetized central IC. E)  
 290 Distribution of iMM in the awake vs. anesthetized shell IC. Bar plots represent means over the population of  $n = 165$  neurons. Error  
 291 bars are standard error of the mean. F) iPE distribution in the awake vs. anesthetized shell IC. G) iRS distribution in the awake vs.  
 292 anesthetized shell IC.

293 (Figure 3D, bottom) and a small amount of prediction error (Figure 3D, middle). Prediction error was  
294 abolished during laser inactivation (Figure 3D, middle; Table 1;  $p=0.048$ , Wilcoxon signed rank test),  
295 while repetition suppression remained unaffected (Figure 3D, bottom). Adapting neurons in shell  
296 regions of IC exhibited a similar pattern to those in the central nucleus. At baseline, these neurons  
297 encoded both prediction error and repetition suppression (Figure 3E, middle and bottom). A  
298 significant decrease in iMM during laser inactivation (Figure 3E, top; Table 1;  $p=0.0023$ , Wilcoxon  
299 signed rank test) was driven by a decrease in prediction error (Figure 3E, middle; Table 1;  $p=0.034$ ,  
300 Wilcoxon signed rank test), whereas repetition suppression remained unaffected (Figure 3E, bottom).  
301 Combined, these results suggest that removing cortical feedback reduced prediction error but not  
302 repetition suppression in adapting neurons.

303 Prior studies of deviance detection in IC have focused exclusively on adapting neurons. However,  
304 given the relative prevalence of facilitating neurons discovered in the awake versus anesthetized IC  
305 (Figure 2), we further investigated this population of neurons to determine whether facilitation reflects  
306 prediction or repetition effects. In the central nucleus, cortico-collicular inactivation led to a  
307 significant decrease in facilitation in facilitating neurons (Figure 3G, top; Table 1;  $p=0.0036$ ,  
308 Student's t-Test). At baseline, the iMM for facilitating neurons represents a combination of negative  
309 prediction error and repetition enhancement (Figure 3G, middle and bottom). During inactivation,  
310 negative prediction error remained unaffected (Figure 3G, middle), while repetition enhancement was  
311 nearly abolished (Figure 3G, bottom; Table 1;  $p=0.0026$ , Student's t-Test). Facilitating neurons in the  
312 shell IC were also significantly affected by cortico-collicular inactivation (Figure 3H, top; Table 1;  
313  $p=0.0016$ , Wilcoxon signed rank test). In this case, however, the change in iMM was driven by the  
314 near abolishment of negative prediction error (Figure 3H, middle; Table 1;  $p=0.037$ , Wilcoxon signed  
315 rank test), while repetition enhancement was unaffected (Figure 3H, bottom).

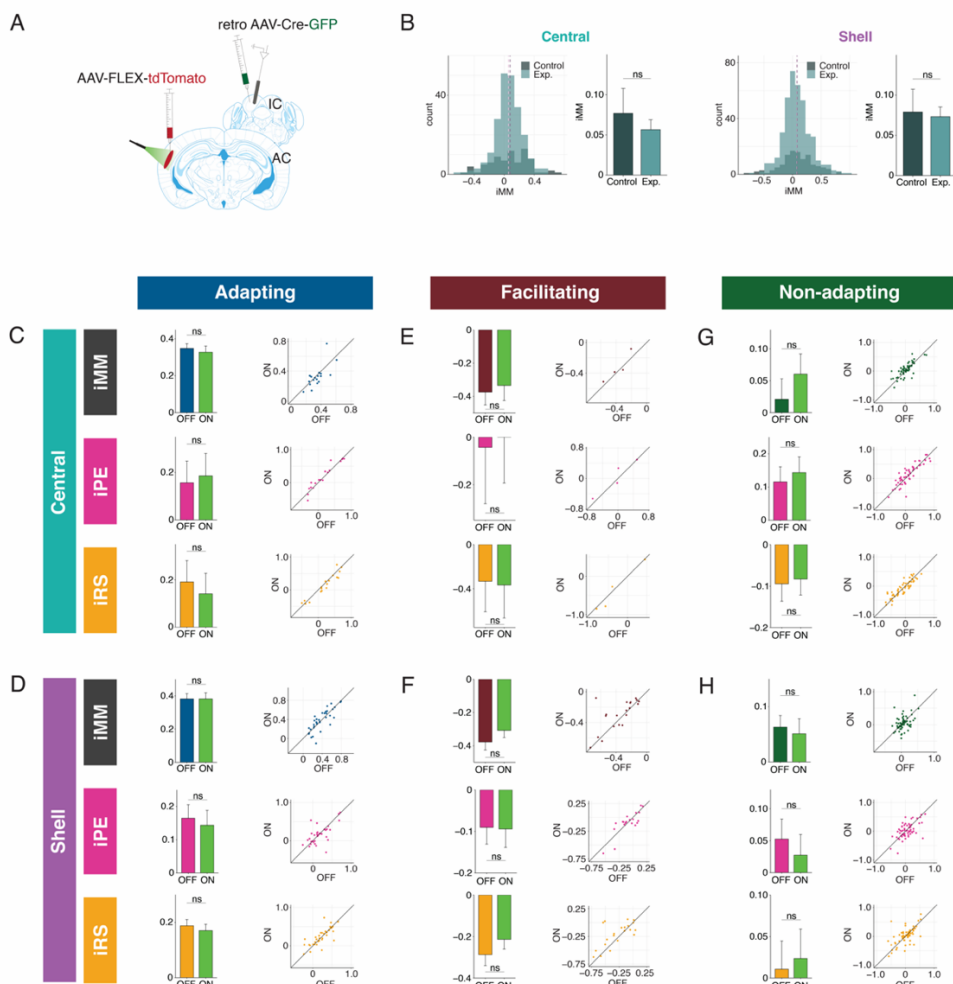
316 These data suggest that adaptation and facilitation in the awake IC are composed of distinct  
317 underlying processes: adapting populations in both central and shell regions of IC exhibit prediction  
318 error and repetition suppression, while facilitating populations are characterized by negative  
319 prediction error and repetition enhancement. In adapting neurons in both central and shell regions,  
320 cortico-collicular inactivation significantly decreases prediction error. Facilitating neurons in the  
321 central IC display decreased repetition enhancement with cortico-collicular inactivation, while those  
322 in shell regions exhibit decreased negative prediction error. To ensure that the laser-induced changes  
323 described above were opsin-mediated, we performed control experiments in two mice with identical  
324 manipulations to the experimental group, but in the absence of ArchT (Figure 3 – Figure Supplement  
325 1A). At baseline, the control group exhibited a similar distribution of iMM values to the experimental



326  
327  
328  
329  
330  
331  
332  
333  
334  
335  
336  
337  
338  
339

Figure 3: Adapting and facilitating IC neurons are differentially affected by cortico-collicular inactivation. A) Experimental design for recording in awake IC during laser inactivation of the cortico-collicular pathway. B) Categorization of neurons according to whether they displayed significant adaptation, facilitation, or neither (non-adapting). C) Average peristimulus time histogram for adapting neurons in central (top) and shell (bottom) IC. Green = during laser inactivation. D) iMM (top), iPE (middle), and iRS (bottom) for adapting neurons in the central nucleus. Dots represent individual neurons. Bar plots represent means over the population of  $n = 52$  neurons. Error bars are standard error of the mean. E) iMM (top), iPE (middle), and iRS (bottom) for adapting neurons in shell regions of IC. Dots represent individual neurons. Bar plots represent means over the population of  $n = 113$  neurons. Error bars are standard error of the mean. F) Average peristimulus time histogram for facilitating neurons in central (top) and shell (bottom) IC. Green = during laser inactivation. G) iMM (top), iPE (middle), and iRS (bottom) for facilitating neurons in the central nucleus. Dots represent individual neurons. Bar plots represent means over the population of  $n = 14$  neurons. Error bars are standard error of the mean. H) iMM (top), iPE (middle), and iRS (bottom) for facilitating neurons in shell regions of IC. Dots represent individual neurons. Bar plots represent means over the population of  $n = 38$  neurons. Error bars are standard error of the mean. This figure has Figure Supplements 1 and 2.

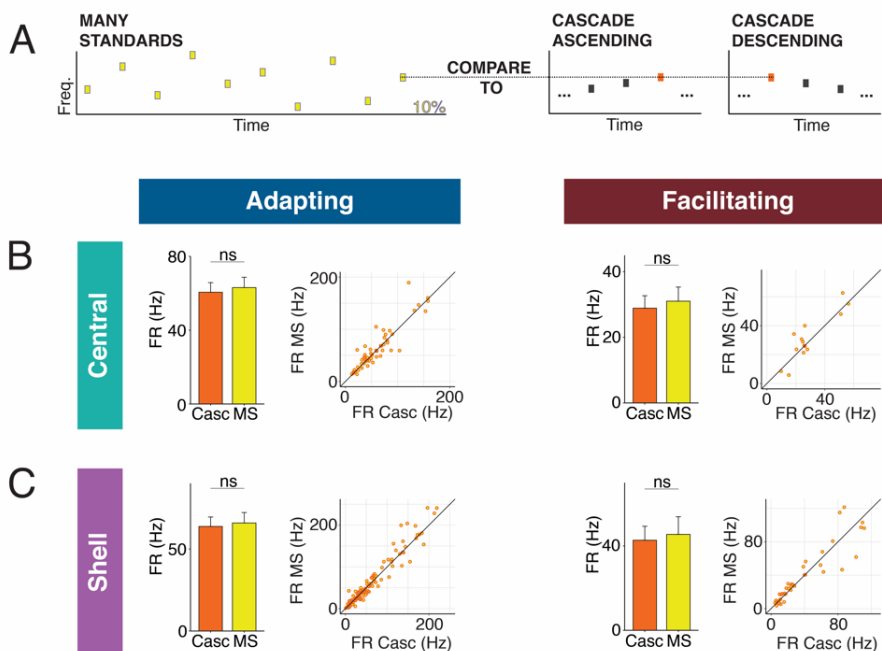
340 group in both the central and shell regions of IC (Figure 3 – Figure Supplement 1B, Table 2). We  
 341 found no significant differences between baseline and laser trials for either adapting (Figure 3 – Figure  
 342 Supplement 1C, D, Table 2) or facilitating (Figure 3 – Figure Supplement 1E, F) neurons in either  
 343 region. This experiment confirmed that the observed effects of cortico-collicular inactivation were  
 344 indeed due to opsin-mediated inactivation of the cortico-collicular projection neurons.  
 345



346  
 347 Figure 3 – Figure Supplement 1: Control data. A) Experimental design for control experiments. All procedures were performed  
 348 identically to the experimental group, except with the omission of ArchT from the viral construct injected in AC. B) Comparison of  
 349 iMM distribution for control (navy) and experimental (light blue) groups in central (left) and shell (right) IC. C) iMM (top), iPE  
 350 (middle), and iRS (bottom) for control adapting neurons in the central nucleus. Dots represent individual neurons. Bar plots represent  
 351 means over the population of n = 18 neurons. Error bars are standard error of the mean. D) iMM (top), iPE (middle), and iRS  
 352 (bottom) for control adapting neurons in shell regions of IC. Dots represent individual neurons. Bar plots represent means over the  
 353 population of n = 35 neurons. Error bars are standard error of the mean. E) iMM (top), iPE (middle), and iRS (bottom) for control  
 354 facilitating neurons in the central nucleus. Dots represent individual neurons. Bar plots represent means over the population of n = 4  
 355 neurons. Error bars are standard error of the mean. F) iMM (top), iPE (middle), and iRS (bottom) for control facilitating neurons in  
 356 shell regions of IC. Dots represent individual neurons. Bar plots represent means over the population of n = 21 neurons. Error bars  
 357 are standard error of the mean. G) iMM (top), iPE (middle), and iRS (bottom) for control non-adapting neurons in the central  
 358 nucleus. Dots represent individual neurons. Bar plots represent means over the population of n = 55 neurons. Error bars are standard  
 359 error of the mean. H) iMM (top), iPE (middle), and iRS (bottom) for control non-adapting neurons in shell regions of IC. Dots  
 360 represent individual neurons. Bar plots represent means over the population of n = 63 neurons. Error bars are standard error of the  
 361 mean.

362 *Adapting and facilitating neurons respond similarly to the cascade and many standards controls*

363 Though the cascade sequence is free of repetition effects between adjacent tone pairs, it does  
364 exhibit global repetition across the entire tone sequence. To assess whether global stimulus regularity  
365 affects the response to the cascade context, we used a shuffled version of the cascade sequence, known  
366 as the “many standards” sequence, as an additional control stimulus (Figure 3 – Figure Supplement  
367 2A). The many standards sequence contains the same 10 tones as the cascade but presented in random  
368 order (Figure 3 – Figure Supplement 2A). This reduces the potential for adaptation across adjacent  
369 frequency channels and also eliminates the global predictability of the stimulus, both of which could  
370 lead to suppression of responses to tones in the cascade context and potentially affect the calculations  
371 of iMM, iPE, and iRS. We compared the responses of adapting and facilitating neurons in both central  
372 and shell regions of IC to tones in the cascade versus the many standards context (Figure 3 – Figure  
373 Supplement 2A). We found no significant differences in firing rates to the cascade versus the many  
374 standards contexts (Figure 3 – Figure Supplement 2B, C, Table 1), suggesting that the global structure  
375 of the cascade sequence does not significantly affect how neurons in IC respond to this stimulus, as  
376 has been shown in other structures (Casado-Román et al., 2020; Parras et al., 2021).



377

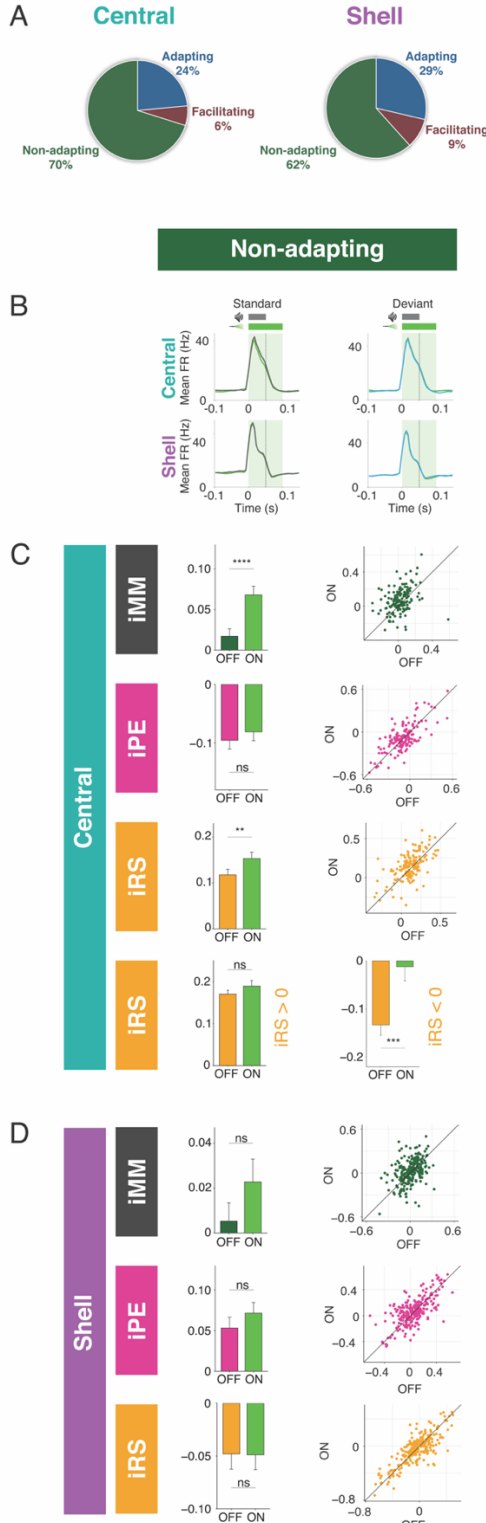
378 Figure 3 – Figure Supplement 2: Comparison of neuronal responses between the many standards and cascade sequences. A) The  
379 many standards sequence consists of the same 10 tones found in the cascade sequence, but the tone order is random. Responses to the  
380 cascade and many standards sequences were compared to assess whether cross-frequency adaptation or global stimulus regularity  
381 affect responses to the cascade condition. B) Firing rates of adapting neurons (left) and facilitating neurons (right) in the central IC to  
382 tones in the cascade and many standards contexts. Dots represent individual neurons. Bar plots represent means over the population  
383 of  $n = 52$  adapting and  $n = 14$  facilitating neurons. Error bars are standard error of the mean. C) Firing rates of adapting neurons (left)  
384 and facilitating neurons (right) in the shell IC to tones in the cascade and many standards contexts. Dots represent individual neurons.  
385 Bar plots represent means over the population of  $n = 113$  adapting and  $n = 38$  facilitating neurons. Error bars are standard error of the  
386 mean.

387 *Non-adapting units also display top-down repetition enhancement*

388 The majority of neurons in both central and shell IC do not exhibit either adaptation or  
389 facilitation but respond similarly to tones when they are presented as a standard or deviant (Figure  
390 4A). However, since both negative and positive metrics are included in the calculation of iMM, it is  
391 still possible that these units exhibit predictive processing that may not be reflected in the overall  
392 iMM value. We further characterized these non-adapting neurons (Figure 4B) and tested how they  
393 are affected by cortico-collicular inactivation. Non-adapting neurons in the central nucleus exhibited  
394 a significant increase in iMM during inactivation (Figure 4C, top; Table 1;  $p=2.7\text{e-}06$ , Wilcoxon  
395 signed rank test), whereas those in the shell IC were unaffected (Figure 4D, top). The change in iMM  
396 for non-adapting neurons in the central nucleus was driven by a significant increase in iRS (Figure  
397 4C, bottom middle; Table 1;  $p=0.0011$ , Wilcoxon signed rank test). To determine whether this  
398 reflected a change in repetition suppression or enhancement, we further segregated central non-  
399 adapting units according to whether their baseline iRS values were negative or positive (Figure 4C,  
400 bottom). Only those units with negative baseline iRS values (i.e., those units showing repetition  
401 enhancement) were significantly affected by cortico-collicular inactivation (Figure 4C, bottom; Table  
402 1;  $p=0.00012$ , Wilcoxon signed rank test). In control experiments without ArchT, no significant  
403 changes were observed in non-adapting neurons (Figure 3 – Figure Supplement 1G, H, Table 2).  
404 These results indicate that, similar to central facilitating units, central non-adapting units display  
405 repetition enhancement, and that input from the cortex is critical for expression of this phenomenon.  
406

407 *Standard and deviant responses are bidirectionally modulated by cortico-collicular inactivation*

408 The observed changes in repetition metrics with cortico-collicular inactivation could reflect  
409 an effect on either the standard or cascade context. Similarly, the shift in prediction metrics observed  
410 with inactivation could be due to altered responses to either the cascade or deviant contexts. We next  
411 determined whether the laser-induced changes in the iMM, the iPE, and the iRS for adapting neurons  
412 reflect changes in the firing rates to the standard, deviant, or cascade contexts. We found that adapting  
413 neurons in the central nucleus increased responses to the standard (Figure 5A, Table 1;  $p=0.0092$ , one  
414 sample t-test) and decreased responses to the deviant (Figure 5A, Table 1;  $p=0.0054$ , one sample t-  
415 test) during inactivation. These results explain the decrease in iMM for this population during the  
416 laser stimulus (Figure 3D, top): the firing rate to the cascade stimulus did not change during cortico-  
417 collicular inactivation, which means that the decrease in firing rate to the deviant alone underlies the  
418 decrease in prediction error observed for this population (Figure 3D, middle). Adapting neurons in  
419 the shell exhibited the same pattern of bidirectional changes to the standard (Figure 5B, Table 1);  
420



421  
422 Figure 4: Non-adapting units also display top-down repetition enhancement. A) Distribution of adapting types (adapting, facilitating,  
423 non-adapting) for neurons in central (left) and shell (right) regions of IC. B) Average peristimulus time histogram for non-  
424 adapting neurons in central (top) and shell (bottom) IC. C) iMM (top), iPE (middle), and iRS (bottom) for non-adapting neurons in  
425 central regions of IC. Dots represent individual neurons. Bar plots represent means over the population of n = 155 neurons. Error bars  
426 are standard error of the mean. D) iMM (top), iPE (middle), and iRS (bottom) for non-adapting neurons in shell regions of IC. Dots  
427 represent individual neurons. Bar plots represent means over the population of n = 243 neurons. Error bars are standard error of the  
428 mean.

429 p=0.035, one sample Wilcoxon test) and deviant (Figure 5B, Table 1; p=0.0057, one sample  
430 Wilcoxon test), similarly accounting for their decrease in iMM and prediction error (Figure 3E), with  
431 no change in response to the cascade condition (Figure 5B). These data suggest that inactivation of  
432 the cortico-collicular pathway induces bidirectional changes in firing rates to the standard and deviant  
433 for adapting neurons in both central and shell regions of IC.

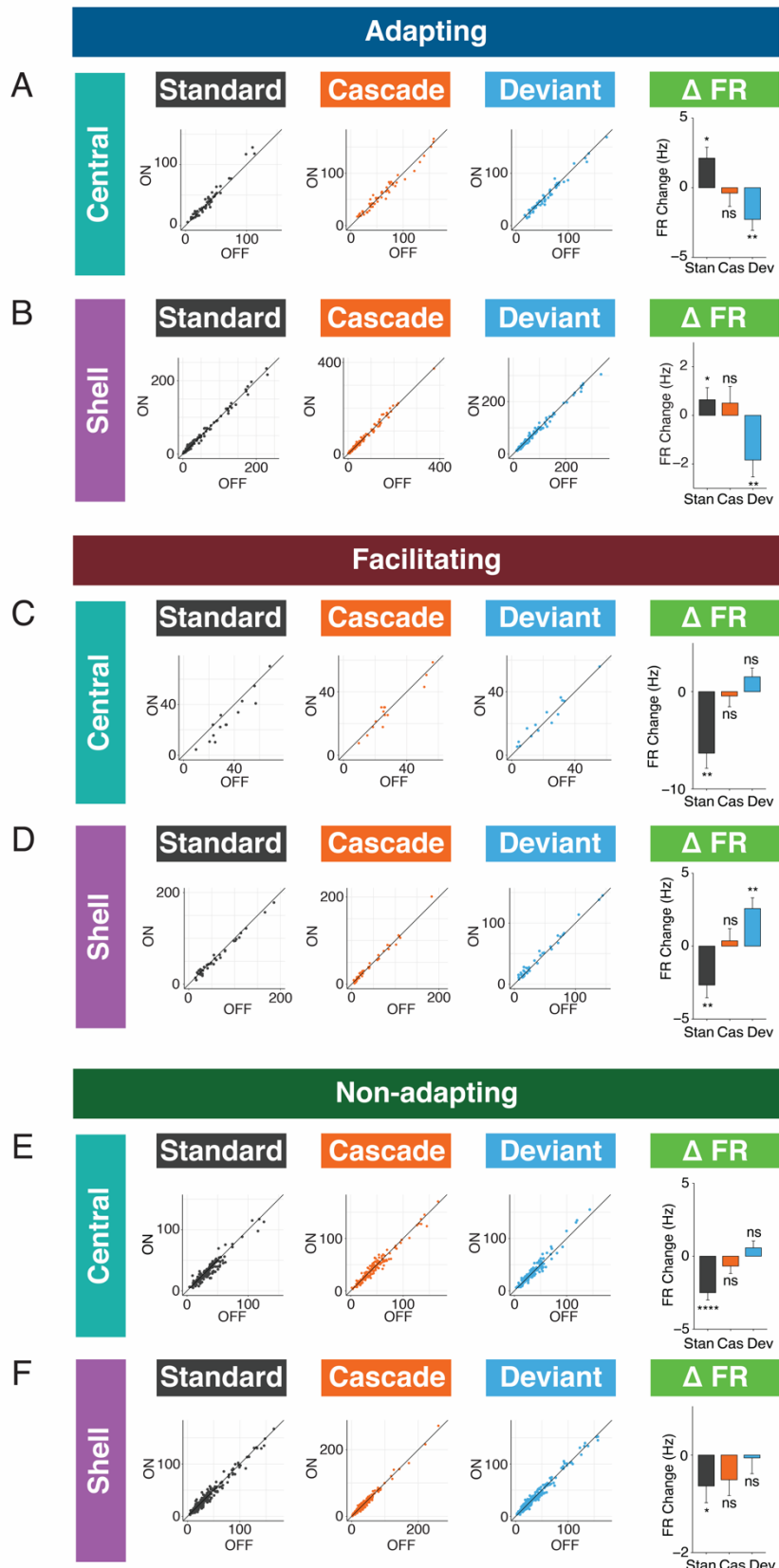
434 We also investigated how responses to each stimulus context changed with cortico-collicular  
435 inactivation for facilitating neurons. For central facilitating neurons, only the firing rate to the  
436 standard context changed during inactivation (Figure 5C, Table 1; p=0.0013, one sample t-test),  
437 explaining the observed change in repetition enhancement for this population (Figure 3G). For shell  
438 facilitating neurons, a decreased response to the standard (Figure 5D, Table 1; p=0.0042, one sample  
439 t-test) and an increased response to the deviant (Figure 5D, Table 1; p=0.0013, one sample t-test)  
440 were elicited on laser trials, accounting for changes in the iMM and the abolishment of negative  
441 prediction error (Figure 3H). These changes are directionally opposite to the observed firing rate  
442 changes observed for adapting neurons under inactivation, with a decrease to the standard context for  
443 both central and shell neurons and an increase to the deviant context for shell neurons.

444 For non-adapting neurons, a significant decrease in response to the standard context was  
445 observed in both central (Figure 5E, Table 1; p=1.4e-06, one sample Wilcoxon test) and shell (Figure  
446 5F, Table 1; p=0.035, one sample Wilcoxon test) regions of IC. The decrease was only significant  
447 enough to produce an effect on the iMM in central regions (Figure 4C, top), leading to an increase in  
448 repetition suppression (Figure 4C, bottom).

449 For adapting and facilitating neurons, these data exhibit that IC responses to the standard and  
450 deviant contexts in the absence of cortical input are bidirectionally modulated, such that neurons  
451 respond more similarly to both contexts rather than firing differentially to each. For non-adapting  
452 neurons, the response to the standard context alone is diminished during cortico-collicular  
453 inactivation, causing these neurons to become more adapting. These changes suggest that under  
454 normal conditions, AC provides information regarding sound context to neurons in IC.  
455

#### 456 *Individual neurons have distinct combinations of iPE and iRS*

457 To determine whether sensitivity to repetition and prediction is encoded in distinct neuronal  
458 populations, or whether individual neurons exhibit particular combinations of repetition  
459 suppression/enhancement and prediction error/negative prediction error, we plotted the iPE values  
460 against the iRS values for each neuron in the adapting, facilitating, and non-adapting groups. Both  
461 the adapting and non-adapting groups in the central IC contained neurons with significant values for

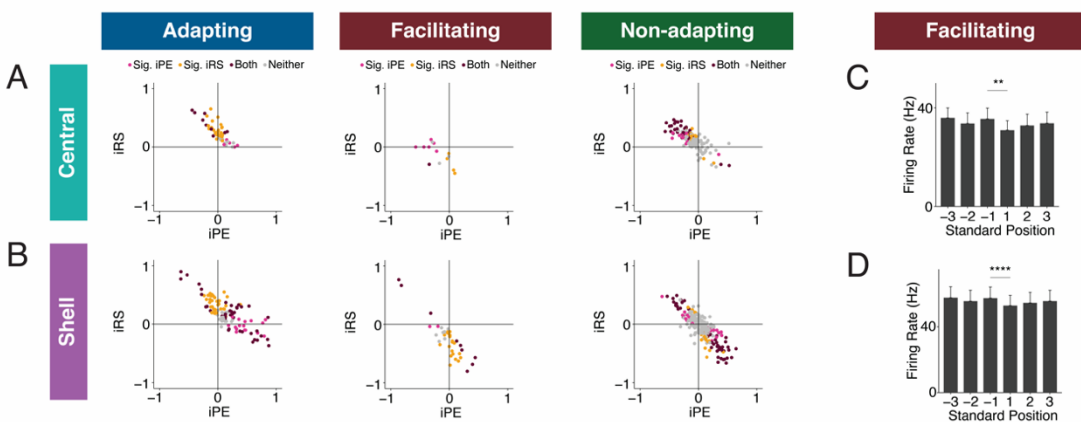


462

463 Figure 5: Standard and deviant responses are bidirectionally modulated by cortico-collicular inactivation. A) Responses to the  
464 standard (left), cascade (middle left), and deviant (middle right) for adapting neurons in central regions of IC under baseline and laser

465 conditions. Change in firing rate between the laser and baseline condition for each stimulus (right). Dots represent individual  
466 neurons. Bar plots represent means over the population of n = 52 neurons. Error bars are standard error of the mean. B) Responses to  
467 the standard (left), cascade (middle left), and deviant (middle right) for adapting neurons in shell regions of IC under baseline and  
468 laser conditions. Change in firing rate between the laser and baseline condition for each stimulus (right). Dots represent individual  
469 neurons. Bar plots represent means over the population of n = 113 neurons. Error bars are standard error of the mean. C) Responses  
470 to the standard (left), cascade (middle left), and deviant (middle right) for facilitating neurons in central regions of IC under baseline  
471 and laser conditions. Change in firing rate between the laser and baseline condition for each stimulus (right). Dots represent  
472 individual neurons. Bar plots represent means over the population of n = 14 neurons. Error bars are standard error of the mean. D)  
473 Responses to the standard (left), cascade (middle left), and deviant (middle right) for facilitating neurons in shell regions of IC under  
474 baseline and laser conditions. Change in firing rate between the laser and baseline condition for each stimulus (right). Dots represent  
475 individual neurons. Bar plots represent means over the population of n = 38 neurons. Error bars are standard error of the mean. E)  
476 Responses to the standard (left), cascade (middle left), and deviant (middle right) for non-adapting neurons in central regions of IC  
477 under baseline and laser conditions. Change in firing rate between the laser and baseline condition for each stimulus (right). Dots  
478 represent individual neurons. Bar plots represent means over the population of n = 155 neurons. Error bars are standard error of the  
479 mean. F) Responses to the standard (left), cascade (middle left), and deviant (middle right) for non-adapting neurons in shell regions  
480 of IC under baseline and laser conditions. Change in firing rate between the laser and baseline condition for each stimulus (right).  
481 Dots represent individual neurons. Bar plots represent means over the population of n = 243 neurons. Error bars are standard error of  
482 the mean.

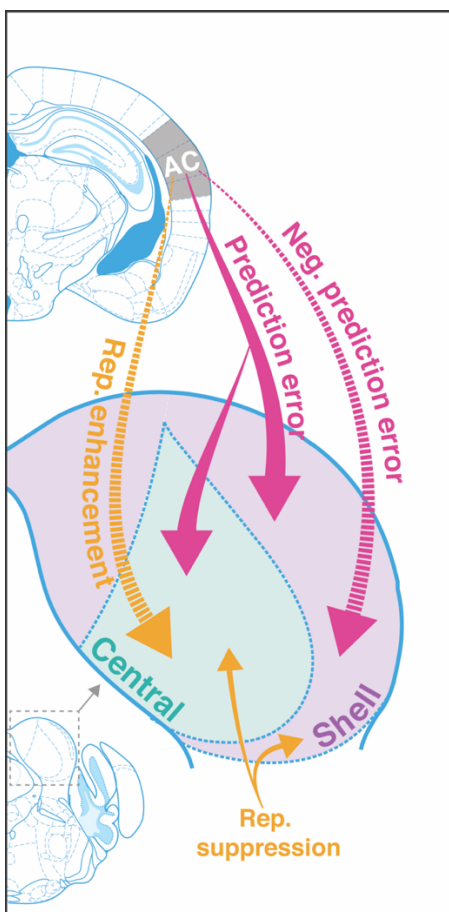
483 both iPE and iRS, most often resulting from a combination of negative prediction error and repetition  
484 suppression (Figure 6A, maroon dots). In the shell IC, a greater variety of response combinations was  
485 observed. All three groups contained neurons with both significant negative prediction error and  
486 repetition suppression, as well as a separate population exhibiting significant prediction error and  
487 repetition enhancement (Figure 6B, maroon dots). Some shell adapting neurons also exhibited a  
488 combination of both repetition suppression and prediction error (Figure 6B, left). These results  
489 suggest that individual neurons in IC exhibit distinct combinations of repetition  
490 suppression/enhancement and prediction error/negative prediction error.



491  
492 Figure 6: Individual neurons exhibit distinct combinations of iPE and iRS. A) Distribution of both iRS and iPE in individual adapting  
493 (left), facilitating (middle), and non-adapting (right) neurons in central IC. B) Plots of distributions of both iRS and iPE in individual  
494 adapting (left), facilitating (middle), and non-adapting (right) neurons in shell IC. C) Response to three subsequent standards prior to  
495 or following the deviant in facilitating neurons in central IC. Comparison between the last standard before and the first standard after  
496 the deviant demonstrates significant repetition enhancement. Bar plots represent means over the population of n = 14 neurons. Error  
497 bars are standard error of the mean. D) Response to three subsequent standards prior to or following the deviant in facilitating  
498 neurons in shell IC. Comparison between the last standard before and the first standard after the deviant demonstrates significant  
499 repetition enhancement. Bar plots represent means over the population of n = 38 neurons. Error bars are standard error of the mean.

500 *Facilitating neurons exhibit true repetition enhancement*

501 Facilitating neurons in both central and shell regions of IC exhibited repetition enhancement  
502 at baseline, as defined by the difference in firing rate to the last standard and the same tone embedded  
503 in the cascade sequence (Figure 3G, 5H). We sought to further characterize the response to the  
504 standard context to determine whether the repetition enhancement captured by the iRS indicates true  
505 repetition enhancement (an incremental increase in firing rate on subsequent presentations of the  
506 standard) or simply a net increase in firing rate to the standard versus cascade condition. We  
507 calculated the mean firing rate for each of the three standards before the deviant and each of the three  
508 standards after the deviant (Figure 6C, 8D). The progression of standards by position exhibited  
509 subsequent enhancements in firing rate that plateaued by the second to last standard before the deviant  
510 for both central (Figure 6C) and shell facilitating neurons (Figure 6D). The firing rate to the last  
511 standard was significantly higher than the first in both regions (Figure 6C, Table 1;  $p=0.0017$ ,  
512 Wilcoxon signed rank test; Figure 6D, Table 1;  $p=9.3e-05$ , Wilcoxon signed rank test). These data  
513 provide evidence that facilitating neurons in IC exhibit true repetition enhancement.



514  
515 Figure 7: Cortico-fugal regulation of predictive coding. Laser inactivation led to the abolishment of repetition enhancement in central  
516 facilitation units and the abolishment of negative prediction error in shell facilitating units. Prediction error decreased during  
517 inactivation for adapting units in both shell and central regions of the IC. Repetition suppression remained unaffected during cortical  
518 inactivation, suggesting that it may reflect fatigue of bottom-up sensory inputs.

519 DISCUSSION

520 *Summary of findings*

521 The results of the present study indicate that AC is critically involved in regulating both  
522 repetition and prediction effects in the awake IC, providing evidence for the implementation of  
523 predictive coding in cortico-subcortical networks. Adapting and facilitating neurons were bi-  
524 directionally modulated by cortico-collicular inactivation, with adapting neurons becoming less  
525 adapting and facilitating neurons becoming less facilitating on laser trials (Figure 3). The decrease in  
526 adaptation for adapting neurons was driven by a decrease in prediction error for neurons in both  
527 central and shell regions of IC (Figure 3D, 5E; Figure 7, pink arrows). For facilitating and non-  
528 adapting neurons in the central nucleus, inactivation-driven changes were caused by a decrease in  
529 repetition enhancement (Figure 3G; Figure 7, gold dashed arrows). The decrease in facilitation in the  
530 shell IC, however, was caused by the abolishment of negative prediction error (Figure 3H; Figure 7,  
531 pink dashed arrows).

532 In adapting neurons, these changes were modulated by an increased response to the standard  
533 and a decreased response to the deviant, while the opposite pattern was true for facilitating neurons  
534 (Figure 5). Overall, these bi-directional changes indicate that, without input from AC, IC responds  
535 more similarly to tones in the standard and deviant contexts. These findings demonstrate that AC  
536 provides critical contextual cues about the statistics of the auditory environment to targets in IC under  
537 normal conditions. We further discuss these results in the context of a hierarchical predictive coding  
538 framework below.

539

540 *iMM in the awake versus anesthetized IC*

541 Our results include the first investigation of how the repetition and prediction processes that  
542 underlie deviance detection in the awake IC compare to the anesthetized condition. Our data suggest  
543 that while iMM values are higher under anesthesia, they almost entirely reflect repetition suppression,  
544 with only a small contribution of prediction error (Figure 2). In the central IC, modest prediction error  
545 is present under anesthesia, but negative prediction error becomes dominant when the animal is  
546 awake. In the shell IC, the same neurons exhibit drastically different iPE and iRS values for the awake  
547 versus the anesthetized condition. Prediction error is substantially higher in the awake IC and  
548 repetition enhancement, rather than repetition suppression, is observed (Figure 2F, 4G). These  
549 findings suggest that the iMM values in the awake and anesthetized brain reflect different underlying  
550 processes, and that anesthesia induces bidirectional changes in metrics of repetition and prediction.

551

552 *Facilitating neurons in IC*

553 We also provide here the first analysis of facilitating neurons in IC. Previous studies that have  
554 investigated iMM have focused selectively on the positive side of the iMM distribution, since these  
555 neurons display adaptation. However, facilitation seems to be enriched in the awake IC (Figure 2B,  
556 4E) and reflects other potentially interesting parameters, such as repetition enhancement (represented  
557 as a higher response to the standard than the cascade sequence) (Figure 2G) and negative prediction  
558 error (represented as a higher response to the cascade than the deviant) (Figure 2C).

559

560 *Repetition enhancement and repetition suppression in IC*

561 Because previous studies that have applied a predictive coding framework to decompose  
562 neuronal mismatch have focused exclusively on adapting neurons, the repetition enhancement found  
563 here in facilitating neurons has not been previously described (Parras et al., 2017). However, it is  
564 well-documented in fMRI literature that repetition enhancement is a common phenomenon in  
565 humans, existing either alongside or in place of repetition suppression (De Gardelle et al., 2013;  
566 Müller et al., 2013; Segaert et al., 2013). Interestingly, repetition enhancement has been proposed to  
567 reflect novel network formation and consolidation of novel sensory representations (Segaert et al.,  
568 2013). Once new representations have been formed, repetition suppression is hypothesized to take  
569 over, reflecting the minimization in prediction errors that occurs when new representations give rise  
570 to accurate predictions (Auksztulewicz & Friston, 2016; De Gardelle et al., 2013; Friston & Kiebel,  
571 2009). Though the repetition enhancement described in human studies differs drastically on spatial  
572 and temporal scales from the phenomenon described here, we find that it similarly involves a  
573 sequential enhancement in the response to subsequent presentations of the standard (Figure 6C, 8D).  
574 Repetition enhancement has also been observed in the medial geniculate body in response to  
575 temporally degraded stimuli that are hypothesized to engage top-down resources to compensate for  
576 bottom-up acoustic information loss (Cai et al., 2016; Kommajosyula et al., 2019). Interestingly, this  
577 enhancement is reversed when cortico-thalamic pathways are blocked, further suggesting that  
578 repetition enhancement in the auditory system reflects a top-down phenomenon (Kommajosyula et  
579 al., 2021).

580 While repetition suppression can be understood from a predictive coding framework, it can  
581 also be viewed from the perspective of neuronal fatigue, whereby the incremental decrease in firing  
582 rate to a repeated standard tone is simply explained by synaptic depression (Escera & Malmierca,  
583 2014; Taaseh et al., 2011). Interestingly, we did not find any effect on repetition suppression during  
584 cortico-collicular inactivation, suggesting that it may reflect fatigue of bottom-up sensory inputs

585 rather than an active predictive process (Figure 3D, 5E; Figure 7, gold arrows). While these data do  
586 not provide definitive proof of either perspective, they do suggest that the processes that underlie  
587 repetition suppression in IC do not involve top-down cortical signals. This notion is supported by the  
588 fact that repetition suppression was much more prevalent when animals were under anesthesia, a state  
589 in which the auditory responsiveness in the cortex is compromised (Figure 2G) (Brugge & Merzenich,  
590 1973; Katsuki et al., 1959).

591

### 592 *Prediction error in IC*

593 In both central and shell populations that exhibited prediction error at baseline, cortico-  
594 collicular inactivation led to a decrease, or complete abolishment, of prediction error (Figure 3D, 5E).  
595 According to models of hierarchical predictive coding, higher-order stations generate predictions that  
596 they broadcast to lower centers (Friston & Kiebel, 2009). These predictions are compared with  
597 representations of the actual sensory input, and if there is a mismatch, a prediction error is generated  
598 and forwarded up the hierarchy (Friston & Kiebel, 2009). Under this framework, the inactivation of  
599 top-down inputs would interfere with communication of predictions, leading to dysfunction in the  
600 prediction error response, as seen in our data. Another possibility is that prediction errors are directly  
601 backpropagated from AC to IC. While this contradicts canonical predictive coding models, evidence  
602 for prediction error has been found in deep layers of the cortex in which feedback neurons reside  
603 (Asilador & Llano, 2020; Rummell et al., 2016). Though the precise mechanism underlying the  
604 generation of prediction error in IC remains unclear, our data show that feedback from AC plays a  
605 critical role in this process.

606

### 607 *Negative prediction error in IC*

608 In addition to neurons with prediction error, we found neurons in IC that responded more  
609 strongly to the cascade than the deviant context (Figure 3G, 5H), consistent with previous reports  
610 (Parras et al., 2017). A stronger response to a tone in the cascade sequence compared to the context  
611 in which it is a deviant could simply reflect a relative lack of cross-frequency adaptation; the oddball  
612 stimulus consists of repeated tone presentations of two neighboring frequencies, making it more likely  
613 to generate cross-frequency effects than the cascade stimulus, which cycles through repetitions of 10  
614 evenly-spaced frequencies (Parras et al., 2017; Taaseh et al., 2011). Previous studies that have  
615 investigated the effective bandwidth for cross-frequency adaptation, however, have found that it  
616 occurs between channels with a frequency separation of a third of an octave or less (Taaseh et al.,  
617 2011). The stimuli used in the present study had a half-octave frequency separation, indicating that

618 cross-frequency effects should be minimized. Therefore, it is unlikely that the negative prediction  
619 error responses observed in the present study simply reflect cross-frequency adaptation to the oddball  
620 stimulus.

621 A stronger response to a tone when it is embedded in a completely predictable sequence, such  
622 as the cascade sequence, than when it is a deviant could also signify that a neuron encodes predictions,  
623 rather than prediction errors. In hierarchical predictive coding, both predictions and prediction errors  
624 are generated at every level of the hierarchy, with prediction errors being forwarded to ascending  
625 sensory centers and predictions being backpropagated (Friston & Kiebel, 2009). In the shell IC, the  
626 region which receives the vast majority of descending cortical input, evidence for negative prediction  
627 error was abolished during cortico-collicular inactivation (Figure 3H), consistent with the notion that  
628 feedback from the cortex may carry predictions to IC (Bajo et al., 2007; Herbert et al., 1991; Saldaña  
629 et al., 1996; Stebbings et al., 2014). Interestingly, negative prediction error in the central nucleus  
630 remained unperturbed during inactivation of cortical feedback (Figure 3G). Given that only a small  
631 fraction of cortico-collicular fibers terminate in the central nucleus, it is likely that it receives  
632 predictions from another source (Bajo et al., 2007; Herbert et al., 1991; Saldaña et al., 1996; Stebbings  
633 et al., 2014). An intriguing potential candidate for this source of predictions could be the shell IC,  
634 given the extensive network of intracollicular connections in IC (Lesicko & Llano, 2020; Saldaña &  
635 Merchań, 1992; Saldaña & Merchán, 2005). Future studies will be required to determine whether the  
636 negative prediction error metric described here captures the type of top-down predictions described  
637 in canonical predictive coding models.

638

### 639 *Technical considerations*

640 One limitation of the present study is that laser inactivation achieved only partial and not  
641 complete inactivation of the cortico-collicular pathway. Given that light itself can have a modulatory  
642 or toxic effect on neurons, these types of optogenetic experiments require a careful titration between  
643 using enough power to substantially affect the population of interest without causing non-specific  
644 light or heat-based perturbations (Tyssowski & Gray, 2019). Though other techniques, such as  
645 chemogenetic approaches or cooling, provide more complete inactivation, they do not allow for rapid  
646 and reversible inactivation (English & Roth, 2015). With our laser power parameters, we found a  
647 mean 60% reduction in firing in putative cortico-collicular neurons at baseline and a 45% reduction  
648 during presentation of pure tone stimuli (Figure 1 – Figure Supplement 1D). This reduction produced  
649 clear effects on repetition and prediction processing in IC, in several cases with the severe reduction  
650 or complete abolishment of certain metrics of deviance detection, such as prediction error and

651 repetition enhancement in the central nucleus and negative prediction error in the shell IC (Figure 3).  
652 The interpretation of these results should bear in mind that they reflect only partial and not complete  
653 inactivation.

654

655 *Conclusions*

656 Our findings indicate that deviance detection and predictive coding in IC involves additional  
657 complexity than has been previously described. We provide here the first description of facilitating  
658 neurons in IC, as well as evidence for the existence of repetition enhancement and negative prediction  
659 error in these neurons. We show that AC regulates these metrics and is also involved in the  
660 generation of prediction error in IC. Repetition suppression is unaffected by inactivation of  
661 cortical input to IC, providing evidence that this process may reflect bottom-up fatigue rather  
662 than top-down predictive processing. These results demonstrate the role of AC in providing  
663 contextual cues about the auditory stream to targets in IC.

664

665 MATERIALS AND METHODS

666 *Animals*

667 We performed experiments in six adult Cdh23 mice (Cdh23tm2.1Kjn/J, JAX: 018399; 4 males and 2  
668 females, age 3-8 months). This mouse line has a targeted point reversion in the Cdh23 gene that  
669 protects against the age-related hearing loss common to C57BL/6 strains (Johnson et al., 2017).  
670 Animals were housed on a reversed 12-hour light–dark cycle with water and food available ad libitum.  
671 All procedures were approved by the University of Pennsylvania IACUC and the AALAC Guide on  
672 Animal Research. We made every attempt to minimize the number of animals used and to reduce  
673 pain or discomfort.

674 *Virus injection*

675 Mice were continuously anesthetized with isoflurane and mounted in a stereotaxic frame. Buprenex  
676 (0.1 mg/kg), Meloxicam (5 mg/kg) and Bupivicane (2 mg/kg) were injected subcutaneously for  
677 preoperative analgesia. We performed small craniotomies bilaterally over AC (-2.6 mm caudal to  
678 Bregma, ±4.3 mm lateral, +1 mm ventral) and IC (-4.96 mm caudal to Bregma, ±0.5 mm lateral, +0.5  
679 mm ventral and -4.96 mm caudal to Bregma, ±1.25 mm lateral, +1.0 mm ventral). A glass syringe  
680 (30-50 µm diameter) connected to a pump (Pump 11 Elite, Harvard Apparatus) was used to inject  
681 modified viral vectors (AAV9-CAG-FLEX-ArchT-tdTomato or AAV9-CAG-FLEX-tdTomato; 750  
682 nL/site; UNC Vector Core) into AC and a retroAAV construct (retro AAV-hSyn-Cre-GFP; 250  
683 nL/site) into IC (Figure 1A, 2A, Figure 3 – Figure Supplement 1A). Large viral injections were  
684 performed to broadly target cortico-collicular neurons throughout all regions of the auditory cortex.  
685 We implanted fiber-optic cannulas (Thorlabs, Ø200 µm Core, 0.22 NA) bilaterally over AC injection  
686 sites (0.4 mm ventral to brain surface) and secured them in place with dental cement (C and B  
687 Metabond) and acrylic (Lang Dental). IC injection sites were covered with a removable silicone plug  
688 (Kwik-Sil). A custom-built headplate was secured to the skull at the midline and a ground-pin was  
689 lowered into a small craniotomy over Bregma. We injected an antibiotic (5 mg/kg Baytril)  
690 subcutaneously for four days postoperatively. Virus injection sites were confirmed postmortem for  
691 all animals included in the study.

692

693 *Extracellular recordings*

694 We performed recordings a minimum of 21 days after virus injection surgeries to allow adequate  
695 travel time for the viral constructs (Figure 1A). Recordings were carried out inside a double-walled  
696 acoustic isolation booth (Industrial Acoustics) or a custom-built table-mounted acoustic isolation

697 booth. For IC recordings, mice were briefly anesthetized to remove the silicone plug over IC virus  
698 injection sites. Following recovery from anesthesia, the headplate was clamped within a custom base  
699 to provide head-fixation. We lowered a 32-channel silicon probe (Neuronexus) vertically into IC  
700 during presentation of broadband noise clicks and monitored sound responses online to confirm  
701 localization within IC (Figure 1A). In a subset of animals, the probe was first coated in a lipophilic  
702 dye (DiD or DiA; Invitrogen) to aid in posthoc reconstruction of recording sites. In each animal, two  
703 recordings were performed per IC (four total recording sessions bilaterally). Following completion of  
704 all IC recording sessions, we recorded the activity of neurons in AC using the same procedure (Figure  
705 1 – Figure Supplement 1B). We performed a square craniotomy (2 mm x 2 mm) over AC and oriented  
706 the probe vertically to the cortical surface (35-degree angle of the stereotaxic arm).  
707 Electrophysiological data were filtered between 600 and 6000 Hz to isolate spike responses and then  
708 digitized at 32 kHz and stored for offline analysis (Neuralynx). For a subset of recordings, the  
709 experimental procedures were repeated while recording from the same units after the animal had been  
710 anesthetized with isoflurane (Figure 2A). We performed spike sorting using Kilosort2 software  
711 (<https://github.com/MouseLand/Kilosort>). Both single and multi-units were included for all analyses  
712 (experimental IC: 50 single units, 354 multi-units; control IC: 17 single units; 111 multi-units;  
713 anesthetized: 10 single units, 129 multi-units; AC: 95 single units, 300 multi-units; putative cortico-  
714 collicular: 9 single units; 11 multi-units).

715

#### 716 *Laser inactivation*

717 We inactivated cortico-collicular neurons using a 532 nm DPSS laser (GL532T3-300, Slocs lasers, 3  
718 mW power at cannula tip or OptoEngine, MGL-III-532, 15 mW power at cannula tip) connected via  
719 optical fibers to the implanted cannulas (Figure 1A, 2C, 2D). Data collected using either laser was  
720 pooled together, as no significant differences were observed in the strength of inactivation in AC  
721 during silence ( $p=0.054$ , Wilcoxon rank sum test) or the presentation of pure tone stimuli ( $p=0.072$ ,  
722 Wilcoxon rank sum test) between the two lasers. Square laser pulses were timed to coincide with tone  
723 onset and lasted for 100 ms. Evidence of inactivation in putative cortico-collicular neurons  
724 (infragranular AC neurons with a minimum 30% reduction in both baseline and sound-evoked  
725 neuronal activity) was confirmed for all animals included in the study.

726

#### 727 *Stimuli*

728 We generated an initial frequency response function from a sequence of 50 pure tones, 1-70  
729 kHz, repeated 20 times at 70 dB SPL in pseudo-random order. This response function was generated

730 online to select suitable frequencies for the oddball stimuli, i.e. frequencies that would fall into the  
731 average response area for neurons in a given recording. Each tone was 50 ms duration (1 ms cosine  
732 squared ramps) with an inter-stimulus interval (ISI) of 200 ms and presentation rate of 4 Hz. A similar  
733 tuning curve stimulus, with 8 amplitude levels (35-70 dB, 5 dB increments) and 5 repetitions, was  
734 used to further characterize the tuning properties of each neuron (Figure 1 – Figure Supplement 2E,  
735 3F).

736 Oddball tone pairs were chosen to fit within the average response area for neurons from a  
737 given recording. Given the prevalence of inhibited regions in the tuning curves, and the fact that this  
738 often led to differences in the response profile of the neuron to each frequency in the oddball tone  
739 pair, the responses to each frequency were analyzed separately (Figure 1 – Figure Supplement 2F).  
740 Oddball stimuli consisted of a frozen sequence of two pure tones (with the same tone parameters as  
741 those used in the initial frequency response functions) with a 90:10 standard-to-deviant ratio and half-  
742 octave frequency separation. The number of standards interleaved between two deviants was  
743 counterbalanced and varied between 3 and 17 standards. The stimuli were divided into blocks (with  
744 the end of a block defined by the presentation of a deviant), and tone type and laser pairings were  
745 alternated on subsequent blocks. For example, on the first block the laser stimulus was paired with  
746 the deviant, on the second block it was paired with the last standard, and the corresponding tones in  
747 the third block served as baseline controls, with no laser stimulus. The number of preceding standards  
748 in the blocks was balanced for all three laser conditions (deviant, last standard, and baseline). Each  
749 block type (laser + standard, laser + deviant, no laser) was presented 45 times and the total number  
750 of tones in each sequence was 1250. Two oddball sequences were created, both with the same frozen  
751 pattern, but with the frequencies of the standard and the deviant switched.

752 Cascade sequences consisted of either an ascending or descending set of 10 evenly log-spaced  
753 (half-octave separation) pure tones (same tone parameters as described above) (Figure 1C). The two  
754 tones used in the oddball sequences were always included as adjacent tones in the cascade sequences,  
755 though their position within the cascade was varied. To generate the many standards control sequence,  
756 we shuffled the cascade sequences using an algorithm that does not allow for repetition of tones of  
757 the same frequency on subsequent presentations.

758

### 759 *Analysis*

760 To distinguish between shell and central IC recording locations, we plotted the best frequency  
761 for each neuron from a given recording against its depth and fit the data with a robust linear regression  
762 model (Figure 1 – Figure Supplement 2B). Additionally, we computed the mean sparsity for all

763 neurons from a given recording site to quantify the sharpness of tuning. The R<sup>2</sup> metric from the linear  
764 fit and the mean sparsity from each recording were used to perform k-means clustering with two  
765 groups. Each recording was assigned to a location (either central or shell) according to the k-means  
766 output, with central sites typically having high sparsity and high R<sup>2</sup> values and shell sites having low  
767 sparsity and low R<sup>2</sup> metrics (Figure 1 – Figure Supplement 2C).

768 Sound response profiles were categorized quantitatively from analysis of the combined  
769 responses to the standard and deviant tones using MATLAB’s “findpeaks” function with a minimum  
770 peak height set to the mean of the baseline period (50 ms before tone onset) +/- 3 standard deviations.  
771 Units that did not display maxima or minima during the tone duration period (0-50 ms) or in the 50  
772 ms after (the “offset window”) were labeled as sound unresponsive and were removed from the  
773 analysis. Units that showed only a single minimum (“inhibited” units) or only a response in the offset  
774 window were similarly removed from the analysis. Units that showed at least one maxima during the  
775 tone duration period were included in the analysis and further categorized as either onset (single  
776 maxima in the first 10 ms after tone onset), sustained (single maximum after the first 10 ms after tone  
777 onset), E-I or I-E (units that displayed both a maximum and minimum during the tone duration  
778 period), biphasic (units that displayed two maxima during the tone duration period), or mixed (units  
779 with greater than 2 maxima and/or minima during the tone response period). It was common for units  
780 to display a response both during the tone duration window and the offset window, and in these cases  
781 a combined response profile was assigned (e.g., onset/offset, sustained/inhibited-offset). Neurons  
782 with only inhibited or offset responses were removed from the data set.

783 Significant adaptation or facilitation for each neuron was assessed with a Wilcoxon rank sum  
784 test between the trial-by-trial firing rates to the standard and deviant on the 45 baseline trials. The  
785 index of neuronal mismatch (iMM), identical to the traditional SSA index, was further deconstructed  
786 into an index of prediction error (iPE) and an index of repetition suppression (iRS) such that iMM =  
787 iPE + iRS. The raw firing rates to the standard, cascade, and deviant conditions were normalized by

788 dividing by the Euclidean norm,  $N = \sqrt{FR_{Dev}^2 + FR_{Casc}^2 + FR_{Stan}^2}$ . The iPE was calculated as  
789 the difference in normalized firing rate to the deviant and cascade conditions ( $iPE = \frac{FR_{Dev}}{N} - \frac{FR_{Casc}}{N}$ ),  
790 while the iRS was calculated as the difference in normalized firing rate to the cascade and standard  
791 conditions ( $iRS = \frac{FR_{Casc}}{N} - \frac{FR_{Stan}}{N}$ ).

792

793 *Statistical analysis*

794 Shapiro-Wilk tests were used to assess normality. For normally distributed data, Student's T-tests  
795 were performed. When the assumption of normality was violated, Wilcoxon rank sum tests were used  
796 for nonpaired data and Wilcoxon signed rank tests were used for paired data. Cohen's d was calculated  
797 as measure of effect size for t-tests. For Wilcoxon tests, the effect size r was calculated as the z statistic  
798 divided by the square root of the sample size.

799

800 ACKNOWLEDGEMENTS

801 The authors thank members of the Geffen laboratory for helpful discussions. This work was  
802 supported by funding from the National Institute of Health grants F32MH120890 to AMHL,  
803 R01DC015527, R01DC014479 and R01NS113241 to MNG, F31DC016524 to CA, and  
804 R01DA044205, R01DA049545 and U01AA025931 to MDB.

805 Table 1: Statistical comparisons for experimental data.

Comparison	Figure	Mean	Median	SD	SEM	CI ( $\pm$ )	Test	Test statistic	N	df	p	Effect size
Response of putative cortico-collicular neurons in silence (laser OFF vs. ON)	1S1D (top)	OFF: 11 ON: 4.1	OFF: 9.0 ON: 3.5	OFF: 8.9 ON: 3.5	OFF: 2.0 ON: 0.78	OFF: 4.2 ON: 1.6	Wilcoxon signed rank test	V = 0	20	NA	1.9e-06	0.88
Response of putative cortico-collicular neurons to pure tones (laser OFF vs. ON)	1S1D (bottom)	OFF: 18 ON: 9.6	OFF: 8.8 ON: 4.3	OFF: 24 ON: 12	OFF: 5.4 ON: 2.7	OFF: 11 ON: 5.6	Wilcoxon signed rank test	V = 0	20	NA	1.9e-06	0.88
iMM central (awake vs. anesthetized)	2B	Aw: 0.050 An: 0.25	Aw: 0.045 An: 0.28	Aw: 0.21 An: 0.49	Aw: 0.024 An: 0.074	Aw: 0.047 An: 0.15	Wilcoxon rank sum test	W = 952.5	Aw: 78 An: 43	NA	8.8e-05	0.36
iPE central (awake vs. anesthetized)	2C	Aw: -0.13 An: 0.077	Aw: -0.11 An: 0.098	Aw: 0.17 An: 0.53	Aw: 0.019 An: 0.081	Aw: 0.038 An: 0.16	Student's T-test	t = -2.5	Aw: 78 An: 43	38	0.017	0.52
iRS central (awake vs. anesthetized)	2D	Aw: 0.18 An: 0.18	Aw: 0.17 An: 0.30	Aw: 0.17 An: 0.56	Aw: 0.019 An: 0.085	Aw: 0.039 An: 0.17	Wilcoxon rank sum test	W = 1444	Aw: 78 An: 43	NA	0.21	0.12
iMM shell (awake vs. anesthetized)	2E	Aw: 0.095 An: 0.27	Aw: 0.090 An: 0.27	Aw: 0.31 An: 0.35	Aw: 0.025 An: 0.022	Aw: 0.050 An: 0.043	Wilcoxon rank sum test	W = 12502	Aw: 147 An: 254	NA	3.5e-08	0.28
iPE shell (awake vs. anesthetized)	2F	Aw: 0.15 An: 0.018	Aw: 0.15 An: -0.0075	Aw: 0.33 An: 0.39	Aw: 0.027 An: 0.025	Aw: 0.053 An: 0.049	Wilcoxon rank sum test	W = 23368	Aw: 147 An: 254	NA	2.6e-05	0.21
iRS shell (awake vs. anesthetized)	2G	Aw: -0.056 An: 0.25	Aw: -0.085 An: 0.29	Aw: 0.36 An: 0.33	Aw: 0.029 An: 0.020	Aw: 0.058 An: 0.040	Wilcoxon rank sum test	W = 9501.5	Aw: 147 An: 254	NA	2.5e-16	0.41
iMM central adapting (laser OFF vs. ON)	3D (top)	OFF: 0.26 ON: 0.21	OFF: 0.24 ON: 0.19	OFF: 0.096 ON: 0.13	OFF: 0.013 ON: 0.019	OFF: 0.027 ON: 0.037	Wilcoxon signed rank test	V = 1083	52	NA	0.00034	0.50
iPE central adapting (laser OFF vs. ON)	3D (middle)	OFF: 0.0077 ON: -0.029	OFF: 0.036 ON: 0.0041	OFF: 0.16 ON: 0.16	OFF: 0.022 ON: 0.022	OFF: 0.043 ON: 0.044	Wilcoxon signed rank test	V = 907	52	NA	0.048	0.28
iRS central adapting (laser OFF vs. ON)	3D (bottom)	OFF: 0.25 ON: 0.24	OFF: 0.24 ON: 0.24	OFF: 0.16 ON: 0.16	OFF: 0.023 ON: 0.022	OFF: 0.046 ON: 0.045	Wilcoxon signed rank test	V = 832	52	NA	0.19	0.18
iMM shell adapting (laser OFF vs. ON)	3E (top)	OFF: 0.34 ON: 0.31	OFF: 0.32 ON: 0.28	OFF: 0.19 ON: 0.20	OFF: 0.017 ON: 0.019	OFF: 0.035 ON: 0.037	Wilcoxon signed rank test	V = 4283	113	NA	0.0023	0.29
iPE shell adapting (laser OFF vs. ON)	3E (middle)	OFF: 0.15 ON: 0.14	OFF: 0.12 ON: 0.10	OFF: 0.30 ON: 0.30	OFF: 0.028 ON: 0.028	OFF: 0.056 ON: 0.056	Wilcoxon signed	V = 3963	113	NA	0.034	0.20

							d rank test				
iRS shell adapting (laser OFF vs. ON)	3E (bottom)	OFF: 0.19 ON: 0.17	OFF: 0.19 ON: 0.16	OFF: 0.24 ON: 0.24	OFF: 0.023 ON: 0.023	OFF: 0.045 ON: 0.045	Paired t-test	t = 1.6	113 2	11	0.11
iMM central facilitating (laser OFF vs. ON)	3G (top)	OFF: -0.32 ON: -0.13	OFF: -0.31 ON: -0.11	OFF: 0.16 ON: 0.19	OFF: 0.042 ON: 0.050	OFF: 0.090 ON: 0.11	Paired t-test	t = -3.5	14	13	0.00 36
iPE central facilitating (laser OFF vs. ON)	3G (middle)	OFF: -0.20 ON: -0.17	OFF: -0.24 ON: -0.20	OFF: 0.20 ON: 0.17	OFF: 0.054 ON: 0.044	OFF: 0.12 ON: 0.095	Paired t-test	t = -1.2	14	13	0.25
iRS central facilitating (laser OFF vs. ON)	3G (bottom)	OFF: -0.12 ON: 0.036	OFF: -0.092 ON: 0.069	OFF: 0.18 ON: 0.24	OFF: 0.049 ON: 0.064	OFF: 0.11 ON: 0.14	Paired t-test	t = -3.7	14 26	13	0.00 1.0
iMM shell facilitating (laser OFF vs. ON)	3H (top)	OFF: -0.29 ON: -0.19	OFF: -0.24 ON: -0.15	OFF: 0.15 ON: 0.16	OFF: 0.024 ON: 0.026	OFF: 0.048 ON: 0.052	Wilcoxon signed rank test	V = 159	38	NA	0.00 16
iPE shell facilitating (laser OFF vs. ON)	3H (middle)	OFF: -0.026 ON: 0.033	OFF: 0.011 ON: 0.023	OFF: 0.26 ON: 0.29	OFF: 0.042 ON: 0.047	OFF: 0.085 ON: 0.096	Wilcoxon signed rank test	V = 227	38	NA	0.03 7
iRS shell facilitating (laser OFF vs. ON)	3H (bottom)	OFF: -0.26 ON: -0.23	OFF: -0.29 ON: -0.23	OFF: 0.32 ON: 0.33	OFF: 0.052 ON: 0.054	OFF: 0.11 ON: 0.11	Wilcoxon signed rank test	V = 254	38	NA	0.09 3
iMM central non-adapting (laser OFF vs. ON)	4C (top)	OFF: 0.022 ON: 0.072	OFF: 0.023 ON: 0.065	OFF: 0.12 ON: 0.14	OFF: 0.0094 ON: 0.011	OFF: 0.019 ON: 0.022	Wilcoxon signed rank test	V = 3419	155	NA	2.7e-06
iPE central non-adapting (laser OFF vs. ON)	4C (middle top)	OFF: -0.096 ON: -0.081	OFF: -0.098 ON: -0.093	OFF: 0.19 ON: 0.19	OFF: 0.015 ON: 0.015	OFF: 0.030 ON: 0.030	Wilcoxon signed rank test	V = 5327	155	NA	0.20
iRS central non-adapting (laser OFF vs. ON)	4C (middle bottom)	OFF: 0.12 ON: 0.15	OFF: 0.12 ON: 0.15	OFF: 0.15 ON: 0.17	OFF: 0.012 ON: 0.013	OFF: 0.024 ON: 0.027	Wilcoxon signed rank test	V = 4224	155	NA	0.00 11
iRS > 0 central non-adapting (laser OFF vs. ON)	4C (bottom)	OFF: 0.17 ON: 0.19	OFF: 0.16 ON: 0.18	OFF: 0.10 ON: 0.15	OFF: 9.1e-03 ON: 0.013	OFF: 1.8e-02 ON: 0.026	Wilcoxon signed rank test	V = 3313	127	NA	0.07 1
iRS < 0 central non-adapting (laser OFF vs. ON)	4C (bottom)	OFF: -0.13 ON: -0.012	OFF: -0.10 ON: -0.017	OFF: 0.11 ON: 0.15	OFF: 0.021 ON: 0.029	OFF: 0.044 ON: 0.060	Wilcoxon signed rank test	V = 30	25	NA	0.00 012
iMM shell non-adapting (laser OFF vs. ON)	4D (top)	OFF: 0.0053 ON: 0.023	OFF: 0.0062 ON: 0.028	OFF: 0.13 ON: 0.16	OFF: 0.0081 ON: 0.010	OFF: 0.016 ON: 0.020	Wilcoxon signed rank test	V = 12765	243	NA	0.07 6
iPE shell non-adapting (laser OFF vs. ON)	4D (middle)	OFF: 0.053 ON: 0.072	OFF: 0.059 ON: 0.061	OFF: 0.21 ON: 0.20	OFF: 0.013 ON: 0.013	OFF: 0.026 ON: 0.026	Wilcoxon signed rank test	V = 13474	243	NA	0.22
iRS shell non-adapting (laser OFF vs. ON)	4D (bottom)	OFF: -0.048 ON: -0.049	OFF: -0.042 ON: -0.041	OFF: 0.23 ON: 0.22	OFF: 0.015 ON: 0.014	OFF: 0.029 ON: 0.028	Wilcoxon signed rank test	V = 14344	243	NA	0.66

FR change standard central adapting	5A	2.1	2.0	5.6	0.78	1.6	One sample t-test	t = 2.7	52	51	0.0092	0.38
FR change cascade central adapting	5A	-0.38	0.67	6.9	0.95	1.9	One sample t-test	t = -0.40	52	51	0.69	0.056
FR change deviant central adapting	5A	-2.3	-2.2	5.6	0.78	1.6	One sample t-test	t = -2.9	52	51	0.0054	0.40
FR change standard shell adapting	5B	0.64	0.89	5.3	0.50	0.98	One sample Wilcoxon test	V = 3760	113	NA	0.035	0.20
FR change cascade shell adapting	5B	0.50	0.44	7.3	0.68	1.4	One sample t-test	t = 0.74	113	112	0.46	0.069
FR change deviant shell adapting	5B	-1.8	-1.3	7.4	0.69	1.4	One sample Wilcoxon test	V = 2040	113	NA	0.0057	0.26
FR change standard central facilitating	5C	-6.3	-7.3	5.8	1.6	3.4	One sample t-test	t = -4.1	14	13	0.0013	1.1
FR change cascade central facilitating	5C	-0.44	-0.89	4.1	1.1	2.4	One sample t-test	t = -0.40	14	13	0.69	0.11
FR change deviant central facilitating	5C	1.5	1.3	3.4	0.92	2.0	One sample t-test	t = 1.7	14	13	0.12	0.45
FR change standard shell facilitating	5D	-2.7	-3.1	5.4	0.87	1.8	One sample t-test	t = -3.1	38	37	0.0042	0.50
FR change cascade shell facilitating	5D	0.36	0.44	5.1	0.84	1.7	One sample t-test	t = 0.43	38	37	0.67	0.070
FR change deviant shell facilitating	5D	2.6	2.7	4.5	0.74	1.5	One sample t-test	t = 3.5	38	37	0.0013	0.57
FR change standard central non-adapting	5E	-2.5	-2.2	6.2	0.50	0.99	One sample Wilcoxon test	V = 2995	155	NA	1.4e-06	0.38
FR change cascade central non-adapting	5E	-0.68	-0.44	6.3	0.51	1.0	One sample t-test	t = -1.3	155	154	0.18	0.11
FR change deviant central non-adapting	5E	0.57	0.0	5.8	0.47	0.93	One sample t-test	t = 1.2	155	154	0.22	0.098
FR change standard shell non-adapting	5F	-0.63	-0.44	5.3	0.34	0.68	One sample Wilcoxon test	V = 11050	= 243	NA	0.035	0.14

FR change cascade shell non-adapting	5F	-0.51	-0.44	5.1	0.32	0.64	One sample Wilcoxon test	V = 12157	243	NA	0.15	0.089
FR change deviant shell non-adapting	5F	-0.059	0.0	5.0	0.32	0.64	One sample t-test	t = -0.18	243	242	0.86	0.012
FR central facilitating (first vs. last standard)	6C	First: 31 Last: 36	First: 29 Last: 31	First: 15 Last: 16	First: 3.9 Last: 4.4	First: 8.5 Last: 9.5	Wilcoxon signed rank test	V = 0	14	NA	0.0017	0.87
FR shell facilitating (first vs. last standard)	6D	First: 53 Last: 57	First: 38 Last: 42	First: 38 Last: 42	First: 6.2 Last: 6.8	First: 13 Last: 14	Wilcoxon signed rank test	V = 92	38	NA	9.3e-05	0.64
FR central adapting (cascade vs. many standards)	3S2B (left)	Casc: 61 MS: 63	Casc: 50 MS: 52	Casc: 38 MS: 40	Casc: 5.2 MS: 5.6	Casc: 10 MS: 11	Wilcoxon signed rank test	V = 595	52	NA	0.39	0.12
FR central facilitating (cascade vs. many standards)	3S2B (right)	Casc: 29 MS: 31	Casc: 26 MS: 28	Casc: 14 MS: 16	Casc: 3.8 MS: 4.3	Casc: 8.2 MS: 9.3	Wilcoxon signed rank test	V = 41	14	NA	0.49	0.19
FR shell adapting (cascade vs. many standards)	3S2C (left)	Casc: 64 MS: 66	Casc: 43 MS: 41	Casc: 61 MS: 68	Casc: 5.7 MS: 6.4	Casc: 11 MS: 13	Wilcoxon signed rank test	V = 2653	113	NA	0.46	0.064
FR shell facilitating (cascade vs. many standards)	3S2C (right)	Casc: 43 MS: 45	Casc: 24 MS: 28	Casc: 41 MS: 52	Casc: 6.6 MS: 8.4	Casc: 13 MS: 17	Wilcoxon signed rank test	V = 264.5	38	NA	0.41	0.14

806

807

Table 2: Statistical comparisons for control data.

Comparison	Figure	Mean	Median	SD	SEM	CI ( $\pm$ )	Test	Test statistic	N	df	p	Effect size
iMM central (control vs. experimental)	3S1B (left)	Con: 0.092 Exp: 0.057	Con: 0.086 Exp: 0.064	Con: 0.16 Exp: 0.18	Con: 0.011 Exp: 0.012	Con: 0.022 Exp: 0.024	Wilcoxon rank sum test	W = 7919	77 (control) 221 (exp.)	NA	0.37	0.052
iMM shell (control vs. experimental)	3S1B (right)	Con: 0.083 Exp: 0.073	Con: 0.069 Exp: 0.053	Con: 0.23 Exp: 0.24	Con: 0.012 Exp: 0.012	Con: 0.023 Exp: 0.024	Wilcoxon rank sum test	W = 22364	119 (control) 394 (exp.)	NA	0.45	0.034
iMM central adapting (laser OFF vs. ON)	3S1C (top)	OFF: 0.35 ON: 0.33	OFF: 0.35 ON: 0.32	OFF: 0.11 ON: 0.15	OFF: 0.026 ON: 0.034	OFF: 0.054 ON: 0.072	Wilcoxon signed rank test	V = 124	18	NA	0.099	0.40
iPE central adapting (laser OFF vs. ON)	3S1C (middle)	OFF: 0.16 ON: 0.19	OFF: 0.10 ON: 0.081	OFF: 0.39 ON: 0.40	OFF: 0.091 ON: 0.094	OFF: 0.19 ON: 0.20	Paired t-test	t = -1.1	18	17	0.30	0.25
iRS central adapting (laser OFF vs. ON)	3S1C (bottom)	OFF: 0.19 ON: 0.14	OFF: 0.24 ON: 0.14	OFF: 0.38 ON: 0.37	OFF: 0.090 ON: 0.087	OFF: 0.19 ON: 0.18	Paired t-test	t = 1.9	18	17	0.077	0.44
iMM shell adapting (laser OFF vs. ON)	3S1D (top)	OFF: 0.38 ON: 0.38	OFF: 0.35 ON: 0.38	OFF: 0.19 ON: 0.22	OFF: 0.032 ON: 0.037	OFF: 0.065 ON: 0.075	Paired t-test	t = -0.0013	35	34	0.992	0.0002

iPE shell adapting (laser OFF vs. ON)	3S1D (middle)	OFF: 0.16 ON: 0.14	OFF: 0.12 ON: 0.15	OFF: 0.24 ON: 0.26	OFF: 0.041 ON: 0.044	OFF: 0.083 ON: 0.090	Paired t-test	t = 0.58	35	34	0.56	0.099
iRS shell adapting (laser OFF vs. ON)	3S1D (bottom)	OFF: 0.22 ON: 0.24	OFF: 0.24 ON: 0.20	OFF: 0.23 ON: 0.22	OFF: 0.040 ON: 0.038	OFF: 0.081 ON: 0.077	Paired t-test	t = -0.78	35	34	0.44	0.13
iMM central facilitating (laser OFF vs. ON)	3S1E (top)	OFF: -0.37 ON: -0.33	OFF: -0.36 ON: -0.37	OFF: 0.15 ON: 0.18	OFF: 0.077 ON: 0.090	OFF: 0.25 ON: 0.29	Paired t-test	t = -1.1	4	3	0.34	0.57
iPE central facilitating (laser OFF vs. ON)	3S1E (middle)	OFF: -0.043 ON: 0.030	OFF: -0.0047 ON: 0.077	OFF: 0.47 ON: 0.45	OFF: 0.24 ON: 0.22	OFF: 0.75 ON: 0.71	Paired t-test	t = -0.93	4	3	0.42	0.47
iRS central facilitating (laser OFF vs. ON)	3S1E (bottom)	OFF: -0.33 ON: -0.36	OFF: -0.49 ON: -0.53	OFF: 0.55 ON: 0.60	OFF: 0.27 ON: 0.30	OFF: 0.87 ON: 0.95	Paired t-test	t = 0.49	4	3	0.66	0.24
iMM shell facilitating (laser OFF vs. ON)	3S1F (top)	OFF: -0.38 ON: -0.31	OFF: -0.32 ON: -0.30	OFF: 0.22 ON: 0.20	OFF: 0.048 ON: 0.043	OFF: 0.10 ON: 0.090	Wilcoxon signed rank test	V = 63	21	NA	0.070	0.40
iPE shell facilitating (laser OFF vs. ON)	3S1F (middle)	OFF: -0.090 ON: -0.094	OFF: -0.11 ON: -0.081	OFF: 0.18 ON: 0.20	OFF: 0.040 ON: 0.044	OFF: 0.083 ON: 0.093	Wilcoxon signed rank test	V = 109	21	NA	0.84	0.050
iRS shell facilitating (laser OFF vs. ON)	3S1F (bottom)	OFF: -0.29 ON: -0.21	OFF: -0.28 ON: -0.15	OFF: 0.24 ON: 0.21	OFF: 0.053 ON: 0.047	OFF: 0.11 ON: 0.097	Paired t-test	t = -1.8	21	20	0.091	0.39
iMM central non-adapting (laser OFF vs. ON)	3S1G (top)	OFF: 0.021 ON: 0.060	OFF: 0.014 ON: 0.050	OFF: 0.24 ON: 0.23	OFF: 0.032 ON: 0.031	OFF: 0.064 ON: 0.063	Paired t-test	t = -1.8	55	54	0.075	0.24
iPE central non-adapting (laser OFF vs. ON)	3S1G (middle)	OFF: 0.12 ON: 0.14	OFF: 0.034 ON: 0.092	OFF: 0.34 ON: 0.35	OFF: 0.046 ON: 0.047	OFF: 0.092 ON: 0.095	Paired t-test	t = -1.2	55	54	0.23	0.16
iRS central non-adapting (laser OFF vs. ON)	3S1G (bottom)	OFF: 0.095 ON: 0.083	OFF: 0.064 ON: -0.072	OFF: 0.31 ON: 0.29	OFF: 0.042 ON: 0.038	OFF: 0.084 ON: 0.077	Paired t-test	t = -0.57	55	54	0.57	0.077
iMM shell non-adapting (laser OFF vs. ON)	3S1H (top)	OFF: 0.063 ON: 0.051	OFF: 0.040 ON: 0.031	OFF: 0.16 ON: 0.22	OFF: 0.021 ON: 0.027	OFF: 0.042 ON: 0.054	Wilcoxon signed rank test	V = 1133	63	NA	0.39	0.11
iPE shell non-adapting (laser OFF vs. ON)	3S1H (middle)	OFF: 0.053 ON: 0.027	OFF: 0.0	OFF: 0.25 ON: 0.26	OFF: 0.031 ON: 0.032	OFF: 0.063 ON: 0.065	Paired t-test	t = 0.88	63	62	0.38	0.11
iRS shell non-adapting (laser OFF vs. ON)	3S1H (bottom)	OFF: 0.011 ON: 0.024	OFF: 0.028 ON: 0.041	OFF: 0.27 ON: 0.28	OFF: 0.034 ON: 0.035	OFF: 0.068 ON: 0.071	Paired t-test	t = -0.43	63	62	0.67	0.054

809 REFERENCES

- 810 Aitkin, L. M., Webster, W. R., Veale, J. L., & Crosby, D. C. (1975). Inferior colliculus. I.  
811 Comparison of response properties of neurons in central, pericentral, and external nuclei of  
812 adult cat. *Journal of Neurophysiology*, 38(5), 1196–1207.
- 813 Anderson, L A, & Malmierca, M. S. (2013). The effect of auditory cortex deactivation on stimulus-  
814 specific adaptation in the inferior colliculus of the rat. *European Journal of Neuroscience*,  
815 37(1), 52–62.
- 816 Anderson, Lucy A, Christianson, G. B., & Linden, J. F. (2009). Stimulus-specific adaptation occurs  
817 in the auditory thalamus. *Journal of Neuroscience*, 29(22), 7359–7363.
- 818 Antunes, F. M., & Malmierca, M. S. (2011). Effect of auditory cortex deactivation on stimulus-  
819 specific adaptation in the medial geniculate body. *Journal of Neuroscience*, 31(47), 17306–  
820 17316.
- 821 Antunes, F. M., Nelken, I., Covey, E., & Malmierca, M. S. (2010). Stimulus-specific adaptation in  
822 the auditory thalamus of the anesthetized rat. *PLoS One*, 5(11), e14071.
- 823 Asilador, A., & Llano, D. A. (2020). Top-down inference in the auditory system: Potential roles for  
824 corticofugal projections. *Frontiers in Neural Circuits*, 14.
- 825 Auksztulewicz, R., & Friston, K. (2016). Repetition suppression and its contextual determinants in  
826 predictive coding. *Cortex*, 80, 125–140.
- 827 Bajo, V. M., Nodal, F. R., Bizley, J. K., Moore, D. R., & King, A. J. (2007). The ferret auditory  
828 cortex: descending projections to the inferior colliculus. *Cerebral Cortex*, 17(2), 475–491.
- 829 Bastos, A. M., Usrey, W. M., Adams, R. A., Mangun, G. R., Fries, P., & Friston, K. J. (2012).  
830 Canonical microcircuits for predictive coding. *Neuron*, 76(4), 695–711.
- 831 Blackwell, J. M., Lesicko, A., Rao, W., De Biasi, M., & Geffen, M. N. (2020). Auditory cortex  
832 shapes sound responses in the inferior colliculus. *eLife*, 9. <https://doi.org/10.7554/eLife.51890>
- 833 Brugge, J. F., & Merzenich, M. M. (1973). Responses of neurons in auditory cortex of the macaque  
834 monkey to monaural and binaural stimulation. *Journal of Neurophysiology*, 36(6), 1138–1158.
- 835 Bulkin, D. A., & Groh, J. M. (2011). Systematic mapping of the monkey inferior colliculus reveals  
836 enhanced low frequency sound representation. *Journal of Neurophysiology*, 105(4), 1785–  
837 1797.
- 838 Cai, R., Richardson, B. D., & Caspary, D. M. (2016). Responses to predictable versus random  
839 temporally complex stimuli from single units in auditory thalamus: impact of aging and  
840 anesthesia. *Journal of Neuroscience*, 36(41), 10696–10706.
- 841 Casado-Román, L., Carbajal, G. V, Pérez-González, D., & Malmierca, M. S. (2020). Prediction

- 842 error signaling explains neuronal mismatch responses in the medial prefrontal cortex. *PLoS*  
843 *Biology*, 18(12), e3001019.
- 844 Chen, C., Rodriguez, F. C., Read, H., & Escabí, M. A. (2012). Spectrot temporal sound preferences  
845 of neighboring inferior colliculus neurons: implications for local circuitry and processing.  
846 *Frontiers in Neural Circuits*, 6, 62.
- 847 De Franceschi, G., & Barkat, T. R. (2020). Task-induced modulations of neuronal activity along the  
848 auditory pathway. *BioRxiv*.
- 849 De Gardelle, V., Waszczuk, M., Egner, T., & Summerfield, C. (2013). Concurrent repetition  
850 enhancement and suppression responses in extrastriate visual cortex. *Cerebral Cortex*, 23(9),  
851 2235–2244.
- 852 Duque, D., & Malmierca, M. S. (2015). Stimulus-specific adaptation in the inferior colliculus of the  
853 mouse: anesthesia and spontaneous activity effects. *Brain Structure and Function*, 220(6),  
854 3385–3398.
- 855 Duque, D., Pérez-González, D., Ayala, Y. A., Palmer, A. R., & Malmierca, M. S. (2012).  
856 Topographic distribution, frequency, and intensity dependence of stimulus-specific adaptation  
857 in the inferior colliculus of the rat. *Journal of Neuroscience*, 32(49), 17762–17774.
- 858 English, J. G., & Roth, B. L. (2015). Chemogenetics—a transformational and translational platform.  
859 *JAMA Neurology*, 72(11), 1361–1366.
- 860 Escera, C., & Malmierca, M. S. (2014). The auditory novelty system: an attempt to integrate human  
861 and animal research. *Psychophysiology*, 51(2), 111–123.
- 862 Fontanini, A., & Katz, D. B. (2008). Behavioral states, network states, and sensory response  
863 variability. *Journal of Neurophysiology*, 100(3), 1160–1168.
- 864 Friston, K. (2009). The free-energy principle: a rough guide to the brain? *Trends in Cognitive  
865 Sciences*, 13(7), 293–301.
- 866 Friston, K., & Kiebel, S. (2009). Predictive coding under the free-energy principle. *Philosophical  
867 Transactions of the Royal Society B: Biological Sciences*, 364(1521), 1211–1221.
- 868 Gaese, B. H., & Ostwald, J. (2001). Anesthesia changes frequency tuning of neurons in the rat  
869 primary auditory cortex. *Journal of Neurophysiology*, 86(2), 1062–1066.
- 870 Han, X., Chow, B. Y., Zhou, H., Klapoetke, N. C., Chuong, A., Rajimehr, R., Yang, A., Baratta, M.  
871 V, Winkle, J., & Desimone, R. (2011). A high-light sensitivity optical neural silencer:  
872 development and application to optogenetic control of non-human primate cortex. *Frontiers in  
873 Systems Neuroscience*, 5, 18.
- 874 Harms, L., Fulham, W. R., Todd, J., Budd, T. W., Hunter, M., Meehan, C., Penttonen, M., Schall,

- 875 U., Zavitsanou, K., & Hodgson, D. M. (2014). Mismatch negativity (MMN) in freely-moving  
876 rats with several experimental controls. *PloS One*, 9(10), e110892.
- 877 Herbert, H., Aschoff, A., & Ostwald, J. (1991). Topography of projections from the auditory cortex  
878 to the inferior colliculus in the rat. *Journal of Comparative Neurology*, 304(1), 103–122.
- 879 Herrmann, B., Henry, M. J., Fromboluti, E. K., McAuley, J. D., & Obleser, J. (2015). Statistical  
880 context shapes stimulus-specific adaptation in human auditory cortex. *Journal of*  
881 *Neurophysiology*, 113(7), 2582–2591.
- 882 Jaramillo, S., Borges, K., & Zador, A. M. (2014). Auditory thalamus and auditory cortex are equally  
883 modulated by context during flexible categorization of sounds. *Journal of Neuroscience*,  
884 34(15), 5291–5301.
- 885 Johnson, K. R., Tian, C., Gagnon, L. H., Jiang, H., Ding, D., & Salvi, R. (2017). Effects of Cdh23  
886 single nucleotide substitutions on age-related hearing loss in C57BL/6 and 129S1/Sv mice and  
887 comparisons with congenic strains. *Scientific Reports*, 7(1), 1–13.
- 888 KATSUKI, Y., MURATA, K., SUGA, N., & TAKENAKA, T. (1959). Electrical activity of cortical  
889 auditory neurons of unanaesthetized and unrestrained cat. *Proceedings of the Japan Academy*,  
890 35(9), 571–574.
- 891 Kommajosyula, S. P., Bartlett, E. L., Cai, R., Ling, L., & Caspary, D. M. (2021). Corticothalamic  
892 Projections Deliver Enhanced-Responses to Medial Geniculate Body as a Function of the  
893 Temporal Reliability of the Stimulus. *BioRxiv*.
- 894 Kommajosyula, S. P., Cai, R., Bartlett, E., & Caspary, D. M. (2019). Top-down or bottom up:  
895 decreased stimulus salience increases responses to predictable stimuli of auditory thalamic  
896 neurons. *The Journal of Physiology*, 597(10), 2767–2784.
- 897 Lesicko, A.M.H., Hristova, T. S., Maigler, K. C., & Llano, D. A. (2016). Connectional modularity  
898 of top-down and bottom-up multimodal inputs to the lateral cortex of the mouse inferior  
899 colliculus. *Journal of Neuroscience*, 36(43). <https://doi.org/10.1523/JNEUROSCI.4134-15.2016>
- 900 Lesicko, Alexandria M H, & Llano, D. A. (2020). Circuit mechanisms underlying the segregation  
901 and integration of parallel processing streams in the inferior colliculus. *Journal of*  
902 *Neuroscience*, 40(33), 6328–6344.
- 903 Malmierca, M. S., Cristaudo, S., Pérez-González, D., & Covey, E. (2009). Stimulus-specific  
904 adaptation in the inferior colliculus of the anesthetized rat. *Journal of Neuroscience*, 29(17),  
905 5483–5493.
- 906 Malmierca, M. S., Izquierdo, M. A., Cristaudo, S., Hernández, O., Pérez-González, D., Covey, E.,

- 908 & Oliver, D. L. (2008). A discontinuous tonotopic organization in the inferior colliculus of the  
909 rat. *Journal of Neuroscience*, 28(18), 4767–4776.
- 910 Müller, N. G., Strumpf, H., Scholz, M., Baier, B., & Melloni, L. (2013). Repetition suppression  
911 versus enhancement—it's quantity that matters. *Cerebral Cortex*, 23(2), 315–322.
- 912 Natan, R. G., Briguglio, J. J., Mwilambwe-Tshilobo, L., Jones, S. I., Aizenberg, M., Goldberg, E.  
913 M., & Geffen, M. N. (2015). Complementary control of sensory adaptation by two types of  
914 cortical interneurons. *Elife*, 4, e09868.
- 915 Nelken, I., & Ulanovsky, N. (2007). Mismatch negativity and stimulus-specific adaptation in animal  
916 models. *Journal of Psychophysiology*, 21(3–4), 214–223.
- 917 Okada, K., Matchin, W., & Hickok, G. (2018). Neural evidence for predictive coding in auditory  
918 cortex during speech production. *Psychonomic Bulletin & Review*, 25(1), 423–430.
- 919 Pakan, J. M. P., Lowe, S. C., Dylda, E., Keemink, S. W., Currie, S. P., Coutts, C. A., & Rochefort,  
920 N. L. (2016). Behavioral-state modulation of inhibition is context-dependent and cell type  
921 specific in mouse visual cortex. *Elife*, 5, e14985.
- 922 Parras, G. G., Casado-Román, L., Schröger, E., & Malmierca, M. S. (2021). The posterior auditory  
923 field is the chief generator of prediction error signals in the auditory cortex. *NeuroImage*,  
924 118446.
- 925 Parras, G. G., Nieto-Diego, J., Carbajal, G. V, Valdés-Baizabal, C., Escera, C., & Malmierca, M. S.  
926 (2017). Neurons along the auditory pathway exhibit a hierarchical organization of prediction  
927 error. *Nature Communications*, 8(1), 1–17.
- 928 Paxinos, G., & Franklin, K. B. J. (2019). *Paxinos and Franklin's the mouse brain in stereotaxic  
929 coordinates*. Academic press.
- 930 Rao, R. P. N., & Ballard, D. H. (1999). Predictive coding in the visual cortex: a functional  
931 interpretation of some extra-classical receptive-field effects. *Nature Neuroscience*, 2(1), 79–87.
- 932 Rauss, K., Schwartz, S., & Pourtois, G. (2011). Top-down effects on early visual processing in  
933 humans: A predictive coding framework. *Neuroscience & Biobehavioral Reviews*, 35(5),  
934 1237–1253.
- 935 Ress, D., & Chandrasekaran, B. (2013). Tonotopic organization in the depth of human inferior  
936 colliculus. *Frontiers in Human Neuroscience*, 7, 586.
- 937 Ruhnau, P., Herrmann, B., & Schröger, E. (2012). Finding the right control: the mismatch  
938 negativity under investigation. *Clinical Neurophysiology*, 123(3), 507–512.
- 939 Rummell, B. P., Klee, J. L., & Sigurdsson, T. (2016). Attenuation of responses to self-generated  
940 sounds in auditory cortical neurons. *Journal of Neuroscience*, 36(47), 12010–12026.

- 941 Saldaña, E., Feliciano, M., & Mugnaini, E. (1996). Distribution of descending projections from  
942 primary auditory neocortex to inferior colliculus mimics the topography of intracollicular  
943 projections. *Journal of Comparative Neurology*, 371(1), 15–40.
- 944 Saldaña, E., & Merchań, M. A. (1992). Intrinsic and commissural connections of the rat inferior  
945 colliculus. *Journal of Comparative Neurology*, 319(3), 417–437.
- 946 Saldaña, E., & Merchán, M. A. (2005). Intrinsic and commissural connections of the inferior  
947 colliculus. In *The inferior colliculus* (pp. 155–181). Springer.
- 948 Schellekens, W., Van Wezel, R. J. A., Petridou, N., Ramsey, N. F., & Raemaekers, M. (2016).  
949 Predictive coding for motion stimuli in human early visual cortex. *Brain Structure and*  
950 *Function*, 221(2), 879–890.
- 951 Schofield, B. R. (2009). Projections to the inferior colliculus from layer VI cells of auditory cortex.  
952 *Neuroscience*, 159(1), 246–258.
- 953 Schumacher, J. W., Schneider, D. M., & Woolley, S. M. N. (2011). Anesthetic state modulates  
954 excitability but not spectral tuning or neural discrimination in single auditory midbrain  
955 neurons. *Journal of Neurophysiology*, 106(2), 500–514.
- 956 Segaert, K., Weber, K., de Lange, F. P., Petersson, K. M., & Hagoort, P. (2013). The suppression of  
957 repetition enhancement: a review of fMRI studies. *Neuropsychologia*, 51(1), 59–66.
- 958 Shipp, S. (2016). Neural elements for predictive coding. *Frontiers in Psychology*, 7, 1792.
- 959 Shipp, S., Adams, R. A., & Friston, K. J. (2013). Reflections on agranular architecture: predictive  
960 coding in the motor cortex. *Trends in Neurosciences*, 36(12), 706–716.
- 961 Stebbings, K. A., Lesicko, A. M. H., & Llano, D. A. (2014). The auditory corticocollicular system:  
962 Molecular and circuit-level considerations. *Hearing Research*, 314.  
963 <https://doi.org/10.1016/j.heares.2014.05.004>
- 964 Stiebler, I., & Ehret, G. (1985). Inferior colliculus of the house mouse. I. A quantitative study of  
965 tonotopic organization, frequency representation, and tone-threshold distribution. *Journal of*  
966 *Comparative Neurology*, 238(1), 65–76.
- 967 Syka, J., Popelář, J., Kvašnák, E., & Astl, J. (2000). Response properties of neurons in the central  
968 nucleus and external and dorsal cortices of the inferior colliculus in guinea pig. *Experimental*  
969 *Brain Research*, 133(2), 254–266.
- 970 Taaseh, N., Yaron, A., & Nelken, I. (2011). Stimulus-specific adaptation and deviance detection in  
971 the rat auditory cortex. *PloS One*, 6(8), e23369.
- 972 Takesian, A. E., Bogart, L. J., Lichtman, J. W., & Hensch, T. K. (2018). Inhibitory circuit gating of  
973 auditory critical-period plasticity. *Nature Neuroscience*, 21(2), 218–227.

- 974 Torii, M., Hackett, T. A., Rakic, P., Levitt, P., & Polley, D. B. (2013). EphA signaling impacts  
975 development of topographic connectivity in auditory corticofugal systems. *Cerebral Cortex*,  
976 23(4), 775–785.
- 977 Tyssowski, K. M., & Gray, J. M. (2019). Blue light increases neuronal activity-regulated gene  
978 expression in the absence of optogenetic proteins. *ENeuro*, 6(5).
- 979 Ulanovsky, N., Las, L., & Nelken, I. (2003). Processing of low-probability sounds by cortical  
980 neurons. *Nature Neuroscience*, 6(4), 391–398.
- 981 Weissbart, H., Kandylaki, K. D., & Reichenbach, T. (2020). Cortical tracking of surprisal during  
982 continuous speech comprehension. *Journal of Cognitive Neuroscience*, 32(1), 155–166.
- 983 Yaron, A., Hershenhoren, I., & Nelken, I. (2012). Sensitivity to complex statistical regularities in rat  
984 auditory cortex. *Neuron*, 76(3), 603–615.
- 985 Yudintsev, G., Asilador, A., Coppinger, M., Nair, K., Prasad, M., & Llano, D. A. (2019).  
986 Connectional heterogeneity in the mouse auditory corticocollicular system. *BioRxiv*, 571711.
- 987 Zhai, X., Khatami, F., Sadeghi, M., He, F., Read, H. L., Stevenson, I. H., & Escabi, M. A. (2020).  
988 Distinct neural ensemble response statistics are associated with recognition and discrimination  
989 of natural sound textures. *Proceedings of the National Academy of Sciences*, 117(49), 31482–  
990 31493.
- 991